J. exp. Biol. (1979), 80, 17–54
With 14 figures
Printed in Great Britain

A NEW APPROACH TO ANIMAL FLIGHT MECHANICS

BY J. M. V. RAYNER†

Department of Applied Mathematics and Theoretical Physics, University of Cambridge

(*Received* 17 *July* 1978)

SUMMARY

The mechanics of lift and thrust generation by flying animals are studied by considering the distribution of vorticity in the wake. As wake generation is not continuous, the momentum jet theory, which has previously been used, is not satisfactory, and the vortex theory is a more realistic model.

The vorticity shed by the wings in the course of each powered stroke deforms into a small-cored vortex ring; the wake is a chain of such rings. The momentum of each ring sustains and propels the animal; induced power is calculated as the rate of increase of wake kinetic energy.

A further advantage of the vortex theory is that lift and induced drag coefficients are not required; estimated instantaneous values of these coefficients are generally too large for steady state aerodynamic theory to be appropriate to natural flapping flight.

The vortex theory is applied to hovering of insects and to avian forward flight. A simple expression for induced power in hovering is found. Induced power is always greater than simple momentum jet estimates, and the discrepancy becomes substantial as body mass increases.

In hovering the wake is composed of a stack of horizontal, coaxial, circular vortex rings. In forward flight of birds the rings are elliptic; they are neither horizontal nor coaxial because the momentum of each ring balances the vector sum of parasite and profile drag and the bird's weight. Total power consumption as a function of flight velocity is calculated and compared for several species. Power reduction is one of the major factors influencing the choice of flight style.

A large body of data is used to obtain an approximate scaling between stroke period and the body mass for birds. Together with relations between other morphological parameters, this is used to estimate the variation of flight speed and power with body mass for birds, and on this basis deviations from allometric scaling can be related to flight proficiency and to the use of such strategies as the bounding flight of small passerines.

1. INTRODUCTION

There has long been a need for a discussion of the mechanics by which an animal achieves flight, which is consistent with aerodynamics and which can be readily related to the animal's morphology. The arguments presented in this paper are an attempt to fill this gap. The theory described here takes account of the unsteadiness

† Present address: Department of Zoology, University of Bristol, Woodland Road, Bristol BS8 1UG, U.K.

of lift and thrust generation by consideration of vortex motions in the animal's wake, and shows how the resulting implications for such quantities as flight power are reflected in variations in animal morphology and flight style. In this respect the use of allometric scaling applied to body dimensions and flight characteristics proves very instructive.

This paper describes all of the biological and physical arguments related to flight aerodynamics which are necessary for the understanding and use of the vortex theory of animal flight which is presented here, together with a discussion of the applications of the theory to several problems in animal flight. Many of the concepts involved require substantial mathematical calculations which are omitted from this discussion, which is intended primarily for the biological reader. If further details of the mathematical arguments are required the reader is referred to two further papers (Rayner (1979*a*) discussing hovering, and Rayner (1979*b*) discussing forward avian flight); these give a much-expanded version of the material in sections 2 and 3 of this paper, but contain little biological discussion.

The theory recognizes that the most important mechanism by which both lift and thrust are generated derives from trailing vortices shed behind an animal's wings, a fact which has been largely neglected in previous models. By considering the distribution of vorticity in the wake of the animal it is possible to determine the increase in wake kinetic energy during a single stroke, and hence the induced power (rate of working to generate lift and thrust). This novel method of analysis dispenses with the use of lift and induced drag coefficients, both associated with wing circulation and wake vorticity, which have been the main sources of uncertainty in previous calculations.

The application to hovering of birds and insects is discussed in section 2. Induced power can be determined accurately if wing-stroke characteristics and body dimensions are known; the other power components, profile and inertial, are found by familiar methods. Avian forward flight is discussed in sections 3–5; the calculation of total power as a function of velocity is a complicated numerical procedure with results that cannot easily be summarized. We discuss the optimum strategy and morphological criteria for particular flight circumstances.

The data required for power calculation can be divided into two groups. Firstly, the morphological parameters, expressing the structural features of the animal: body mass M, wing semi-span b, maximum wing chord c_0, total wing area S, and the total masses m_p, m_s of a bird's m. pectoralis major and m. supracoracoideus (these masses are only used in relation to avian forward flight; no equivalent measurements are needed for insects). We define two further morphological parameters familiar from aerodynamics: the aspect ratio,

$$A_r = 4b^2/S, \tag{1}$$

which has no dimensions, and the disc loading,

$$N_d = Mg/\pi b^2. \tag{2}$$

As all quantities are in MKS units, N_d is in N m^{-2}. We also need the wing chord distribution $c(\zeta)$ for a bird's wing; Oehme & Kitzler (1975*a*) have shown in a wide range of species that this conforms closely to $c(\zeta) = c_0\bar{c}(\zeta)$, where

$$\bar{c}(\zeta) = \begin{cases} 1 & (0 \leqslant \zeta \leqslant \tfrac{1}{2}), \\ 4\zeta(1-\zeta) & (\tfrac{1}{2} \leqslant \zeta \leqslant 1), \end{cases} \tag{3}$$

with ζ the radial position on either wing moving out from the root. This equation leads to the relation $S = \frac{2}{3}bc_0$, from which we can determine c_0 if b and S are known.

The kinematic parameters describe the geometry of the wing stroke. Stroke period T is determined largely by the animal's morphology (see section 5) and in some senses can be regarded as a morphological parameter. The other data used are the downstroke ratio τ (downstroke duration is τT), stroke plane angle γ (inclination of the plane containing the leading edges of the wings to the horizontal) and the stroke amplitude ϕ. The various parameters are illustrated diagrammatically in Fig. 1; the notation used is listed in Table 1. Data are widely available in the literature (e.g. Weis-Fogh (1973) for insects, Greenewalt (1962) for morphology of insects and birds). We assume throughout that the leading edges of the wings remain straight, rigid and coplanar during the powered portions of the wing beat.

The aim of the theory developed here is to make an accurate estimate of aerodynamic power consumption by flying animals consistent with the fluid dynamics of lift and thrust generation. The majority of existing flight models are also intended to calculate power, and have their origin in the division of power components used in classical aerodynamics: induced power to generate lift, and parasite power to overcome drag. When the wings are beating we must also include the inertial work done by the muscles (inertial power) and the profile power overcoming form and friction drag of beating wings. It is usual to refer to parasite drag as the effect of the animal's body alone. Induced power can be considered either as the rate of working for the wings to overcome induced drag (in which case either the induced drag coefficient or

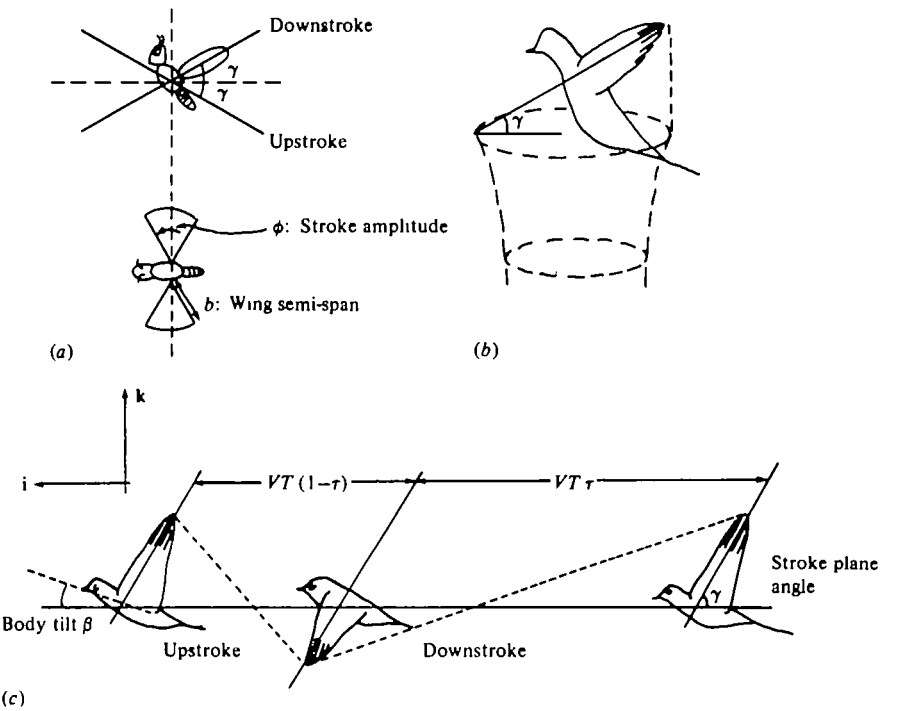

Fig. 1. Diagrammatic view of flying animals. (*a*) Normal hovering of insects and hummingbirds; note that upstroke and downstroke are symmetrical. (*b*) Avian hovering, showing downstroke wingtip path. (*c*) Avian forward flight. Notation is listed in Table 1.

Table 1. *Symbols and notation*

(All physical quantities are given in MKS units.)

		Units
A_r	Aspect ratio	
b	Wing semi-span (length of one wing)	m
C_D, etc.	Drag coefficients, defined in text	
c_0	Maximum wing chord	m
$\bar{c}(\zeta)$	Shape of wing as function of radius	
$\mathbf{D}_{par}$	Parasite drag of body	N
$\mathbf{D}_{pro}$	Total mean profile drag of wings	N
f	Feathering parameter (see (7))	
g	Gravitational acceleration = 9·81 m s^{-2}	
$\mathbf{i}, \mathbf{j}, \mathbf{k}$	Unit vectors	
M	Body mass (body + wings)	kg
m_p, m_s	Masses of m. pectoralis and m. supracoracoideus	kg
N_d	Disc loading	N m^{-2}
P	Flight power	W
P_a	Maximum muscular power output (power available)	W
$P_{i,M}$; $P^*_{i,M}$	Induced power momentum jet; specific induced power	W, W kg^{-1}
P_i	Induced power	W
P_{par}, P_{pro}	Parasite, profile powers	W
R'	Non-dimensional vortex ring radius	
S	Wing area (both wings)	m^2
T	Stroke period	s
T_w	Wake period	s
u_i, u_t	Mean induced fluid velocity, mean tip velocity	m s^{-1}
V	Flight velocity	m s^{-1}
β	Body tilt angle	
γ	Stroke plane angle	
ζ	Non-dimensional wing radius	
θ	Angular position of wing	
μ	Muscle ratio = $1+m_s/m_p$	
ρ	Air density = 1·22 kg m^{-3}	
τ	Downstroke ratio	
ϕ	Stroke amplitude	

some knowledge of the circulation distribution is essential) or as the rate of working generating wake momentum whose reaction sustains and propels the bird. Osborne (1951) formulated the problem of insect flight in this way, and used an estimate of mean induced downwash to replace the induced drag coefficient in his power estimates. Weis-Fogh (1972, 1973) discussed hovering with a similar formulation, using the actuator disc and momentum jet theories. The momentum jet is a powerful technique for the consideration of hovering flight; it is discussed in greater detail in Rayner (1979*a*), section 2.

Pennycuick (1968) gives a theory for power consumption in forward avian flight. Induced power is calculated from a version of the momentum jet theory; the total mass flow through the actuator disc includes the effect of the bird's forward velocity, so that the induced velocity required to sustain and propel the bird decreases as flight velocity V increases. Induced power decays as V^{-1} at large speeds. This approach is unsatisfactory because it treats lift and thrust generation separately; these are the result of the same fluid motions and must be considered together. This is only one of a number of reasons why the momentum jet is inappropriate in forward flight, which are discussed in section 3. Pennycuick also uses the induced downwash to estimate local induced drag in his calculation of profile power, so that work done against

induced forces is included twice in the total power consumption; his estimates of profile power are considerably too high at low velocities, and the deduction that profile power is independent of flight speeds is false. Modifications and extensions to Pennycuick's theory have extended its efficacy (Pennycuick, 1969; Tucker, 1973; Pennycuick, 1975), but it remains an empirical method designed to correspond with alternative power measurements. It has been widely applied in the study of avian forward flight (e.g. Greenewalt, 1975; Oehme, Dathe & Kitzler, 1977; Rayner, 1977; Withers & Timko, 1977), and the basic structure is the foundation of the model given here.

The main deficiencies of Weis-Fogh's and of Pennycuick's power estimates stem from the lack of consideration given to the unsteady nature of the airflow. In most problems concerned with active animal flight the time-scales of the air motions and of the wing beats are similar, and it *cannot* be assumed that the wings operate under steady state conditions. Most simple theories have assumed that the wings operate as quasi-steady aerofoils. There is considerable evidence that many animals in hovering or slow forward flight require mean lift coefficients far in excess of the values their wings could produce in a steady air flow (Weis-Fogh, 1973; Norberg, 1975, 1976*a*, *b*; Hummel & Möllenstädt, 1977; Rayner, 1979*b*, section 5). There are as yet few suggestions as to the mechanisms by which high lift coefficients are obtained; circulation generation and control will be aided by surface features of a bird's wings (Alula, primary feather separation, etc.), and possibly also by the Weis-Fogh 'clap-and-fling' (Lighthill, 1973; Weis-Fogh, 1973). This last is now known to apply in the case of many insects (Cooter & Baker, 1977) and several bird species; high levels of circulation are generated by fluid mass conservation between rapidly opening wings, and are probably retained around the wings without separating destructively by a separation bubble at the leading edge. However, this device cannot help the pied flycatcher (Norberg, 1975), since at all times in a sequence of hovering observations the animal's wings remained at least 70° apart; the mean lift coefficient of 5·3 for the downstroke alone is at least three times greater than steady state aerodynamic theory can allow. There must remain mechanisms appropriate to a reciprocating wing which would benefit from detailed aerodynamic study; it is not the purpose of this work to consider such mechanisms, but merely to describe a procedure based on the fluid flow distribution in the wake which is independent of assumptions about the steadiness of the flow field around the wings, and which moreover does not require the estimation of coefficients of lift or induced drag.

The forces sustaining and propelling any flying animal are the reaction of the momentum contained in fluid flows around the animal, and these flows must be generated by the animal's wing motions alone. The rate of increase of momentum in the wake must equal the lifting and thrusting forces required. The flows generated by the wings are referred to as induced flows. The rate of working by the bird to generate the induced flow, which must equal the rate of increase of the fluid's kinetic energy, is defined as the induced power. It is important to note that the induced flows have non-zero total momentum, and occur away from any bodies in the fluid. Although they must be generated at a solid surface (the animal's wings) they persist in the absence of any boundaries. Flows of this kind are only possible if there is a distribution of vorticity, possibly localized, throughout the fluid. Vorticity (a measure of the local

rotation of the flow field) can only be passed into a fluid at a solid boundary, in our case the animal's wings; *no wing can generate lift without vorticity being present in its wake.*

A line which is everywhere parallel to the local vorticity vector in the fluid is defined as a vortex line. The effect of an isolated line of vorticity can be likened to that of a thin rotating cylinder. If a rotating cylinder is exposed to a fluid velocity in a plane perpendicular to its axis the cylinder experiences a force to the side; this is the mechanism (Magnus effect) by which an aerofoil generates lift. Although vorticity can be distributed arbitrarily throughout a region, there are two configurations which commonly occur in fluid dynamics which are simpler both to visualize and to analyse. In a *vortex sheet* all the vortex lines lie in a thin surface; this is characteristic of the flow immediately behind an aerofoil. A vortex sheet is usually unstable; that behind an aircraft's wing deforms (rolls up) rapidly into a pair of concentrated line vortices. Two theorems about vortex motion state that vortex lines must form closed loops, and that vorticity cannot be destroyed without interacting with a surface (assuming that viscosity is negligible). The strength of the two line vortices must be identical to the total vortex strength in the sheet from which they were formed, and these two vortices must complete a loop with the bound vortex line on the aircraft's wing and with a starting vortex formed where the wing first began to move. The other useful vortex distribution is the *vortex ring*. Here, all vortex lines form similar closed loops azimuthally within a torus, generally taken to have small cross-sectional area. Usually a vortex ring is plane and circular, and then the most familiar example is the smoke ring, but this is not necessarily so. However, if it is of any other shape it cannot persist with shape unchanged.

We can determine the momentum of a distribution of vortex elements by modelling each element by a vortex loop, and calculating the sum of the momenta of all the loops. Momentum is the product of the vortex strength (circulation), the fluid density and the vector area of the loop. By the energy of a vortex distribution we refer to the kinetic energy of the fluid flow which it induces; this can usually be calculated, albeit with some difficulty. Further information on vorticity can be found, for instance, in Batchelor (1967, sections 2.3, 2.6 and 7.1–8).

By analogy with the vortex wake of an aircraft wing, the wings of an animal in flapping flight will shed a vorticity distribution of a complicated twisted shape. The procedure used in this model is to assume that the vorticity shed by *each* wing stroke deforms into a small-cored vortex ring of simple shape. The time evolution of the wake is determined by the interaction of the vortex rings with each other. Induced power is then simply the mean rate of increase of the kinetic energy of this wake. Energy expended as parasite, profile and inertial power is passed to a viscous wake behind the body and wings. This argument is applied to the hovering flight of birds and insects (section 2) and to the forward flight of birds (sections 3–5).

2. HOVERING FLIGHT

The application of the vortex ring theory to hovering involves lengthy numerical calculations, which are described in detail in Rayner (1979*a*). From the results of these calculations we can derive a simple formula which permits us to estimate induced

power for a hovering animal from the minimum of data. The problem can be expressed in such a way that two dimensionless parameters are sufficient to determine wake geometry and power consumption; one of these depends on the wingbeat kinematics (R', initial vortex ring radius) and the other (f, feathering parameter) on morphology.

We can distinguish between two types of wing motions in hovering (Figs. 2*a*, *b*). In *normal* hovering the up and down strokes are symmetrical, with the wingtips moving in a figure of eight; the stroke plane angle is defined as the angle between either branch of this curve and the horizontal. It is typical of the insects and the hummingbirds, excepting those four-winged insects (e.g. Odonata) which beat their wings out of phase and are not considered here. In *avian* hovering (of those birds and bats which can hover, excepting the hummingbirds) the upstroke is feathered and produces little or no useful aerodynamic force (Brown, 1963; Norberg, 1975). The theory described here is equally applicable to both types of hovering. We define the wake period T_w as the period between successive powered strokes; in normal hovering $T_w = \frac{1}{2}T$, and in avian hovering $T_w = T$.

The feathering parameter is defined as the square of the ratio between mean induced velocity past the wings and mean wingtip velocity. The momentum jet theory gives mean induced downwash u_i as

$$u_i = \sqrt{(Mg/2\pi\rho b^2)}, \tag{4}$$

which will be a measure of the magnitude of the true induced velocity on the wing disc; we define mean wingtip velotity u_t as

$$u_t = \pi b/T_w. \tag{5}$$

By the above definition, feathering parameter

$$f = (u_i/u_t)^2, \tag{6}$$

so that we may write

$$f = \frac{MgT_w^2}{2\pi^3 r b^4}. \tag{7}$$

Sample values of f, together with data for the birds and insects we consider, are given in Table 2(*a*) and (*b*).

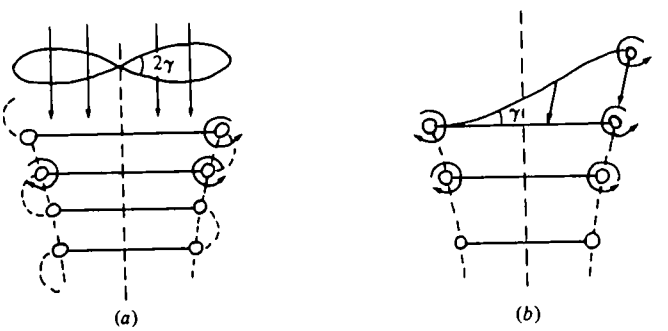

Fig. 2. Diagrammatic representation of formation of vortex ring wake in (*a*) normal hovering and (*b*) avian hovering. Note that self convection of part-formed rings combined with tilted stroke plane results in net vertical wake momentum in both cases.

Table 2. (*a*) *Morphological parameters for animals using normal hovering*

(Data after Weis-Fogh (1973). MKS units throughout.)

	Body mass M (kg)	Wing semi-span b (m)	Disc loading N_d (N m^{-2})	Stroke period T (s)	Feathering parameter, f
Chalcid wasp, *Encarsia formosa*	$2{\cdot}5 \times 10^{-9}$	7×10^{-4}	0·16	1/370	0·025
Fruit-fly, *Drosophila virilis*	2×10^{-6}	3×10^{-3}	0·69	1/240	0·014
Crane-fly, *Tipula paludosa*	$2{\cdot}8 \times 10^{-5}$	0·0173	0·29	1/53	0·0036
Hover-fly, *Eristalis tenax*	$1{\cdot}5 \times 10^{-4}$	0·0127	2·90	1/182	0·0056
Bumble bee, *Bombus terrestris*	$8{\cdot}8 \times 10^{-4}$	0·0173	9·18	1/156	0·013
Moth, *Manduca sexta*	$1{\cdot}12 \times 10^{-3}$	0·050	1·40	1/29·1	0·0069
Hummingbirds					
Amazilia fimbriata	$5{\cdot}1 \times 10^{-3}$	0·059	4·57	1/35	0·011
Patagona gigas	0·02	0·13	3·70	1/15	0·010

We find that the entire problem of the hovering wake can be non-dimensionalized, and all variables are then dependent on the two parameters, f and R'. All physical quantities are expressed as proportions or multiples of a base quantity of the same dimensions, for instance all times in terms of T_w, all lengths in terms of wing semi-span, all velocities in terms of u_i or u_t. Mathematically, this procedure has the benefit of greatly simplifying the calculation and reducing the amount of computation time needed. It also has the great benefit of highlighting the various combinations of dimensional parameters which determine the solution; in our case f is extremely important, and is the only dimensionless number based on flight parameters which enters the hovering flight problem. In forward flight we might also introduce aspect ratio (1) and the ratio of flight speed V to u_t to assist in the analysis of a rather more complex problem. The topic of dimensional analysis of animal locomotion can be found discussed in detail in the various papers contained in Pedley (1977).

The usual method of calculating induced power in hovering is the momentum jet generated by an actuator disc (Hoff, 1919; Weis-Fogh, 1972; Ellington, 1978; Rayner, 1979*a*); the actuator disc is usually assumed to be the wing disc. The momentum jet induced power $P_{i,M}$ is given by (see, for example, Rayner (1979*a*), section 2, (12))

$$P_{i,M} = Mg\sqrt{(Mg/2\pi\rho b^2)}, \tag{8}$$

or

$$P_{i,M} = Mg\sqrt{(N_d/2\rho)}, \tag{9}$$

where N_d is the disc loading. The other components of flight power, profile and inertial, can be calculated by the method of Weis-Fogh (1973) in normal hovering. In avian hovering, profile power is given by equation (39) of Rayner (1979*b*), and inertial power is negligible; parasite power is also negligible.

The actuator disc and momentum jet approach is a good empirical method of deriving power, but has a number of faults which encourage us to investigate further the wake dynamics. Thse faults become more pronounced as f increases, and are certainly significant in avian hovering. The momentum jet theory assumes that momentum is passed steadily into the wake (not consistent with a reciprocating wing beat), that pressure is evenly distributed across the actuator disc, and that all vorticity

Table 2. (*b*) *Morphological data for birds*

(Source of data indicated in the right-hand column, unless individual measurement obtained from elsewhere.)

	Mass M (kg)	Wing semi-span b (m)	Wing area, S (m^2)	Pectoralis major relative mass, m_p/M	Muscle ratio, μ	Stroke period, T (s)	Feathering parameter, f	Aspect ratio, A_r	Disc loading, N_d ($N\ m^{-2}$)	Source*
Wren, *Troglodytes troglodytes*	0·010	0·085	0·0041	0·12	1·1	0·084 (*f*)	0·175	7·0	4·3	(*a*)
Pied flycatcher, *Ficedula hypoleuca*	0·012	0·115	0·0090	0·16 (*a*)	1·1 (*a*)	0·07	0·044	5·9	2·8	(*b*)
Common tern, *Sterna hirundo*	0·118	0·414	0·056	0·16	1·1	0·242 (*g*)	0·031	12·2	2·1	(*a*)
Kestrel, *Falco tinnunculus*	0·245	0·369	0·071	0·12	1·06	0·180 (*c*)	0·056	7·7	5·6	(*a*)
Pigeon, *Columba livia*	0·333	0·316	0·063	0·19	1·1	0·15 (*c*)	0·097	6·3	10·4	(*d*)
Mallard, *Anas platyrhynchos*	1·105	0·450	0·090	0·19	1·15	0·15 (*c*)	0·079	9·0	17·0	(*a*)
Pheasant, *Phasianus colchicus*	1·660	0·425	0·156	0·19 (*a*)	1·15 (*a*)	0·15 (*e*)	0·148	4·6	28·7	(*j*)
Long-eared bat, *Plecotus auritus*	0·009	0·135	0·0123	0·14	?	0·088	0·027	5·9	1·5	(*h*)

* (*a*) Greenewalt (1962); (*b*) Norberg (1975); (*c*) Oehme & Kitzler (1974); (*d*) Oehme & Kitzler (1975*b*); (*e*) Fullerton (1911); (*f*) author's estimate based on allometric scaling; (*g*) Cone (1968); (*h*) Norberg (1976*b*); (*j*) author's measurements.

is confined to the boundary of the wake. It also needs the assumption that within the vortex sheet forming the wake boundary fluid mass and momentum are conserved. These various assumptions give the results (4) and (8) for velocity and power, and also imply that the far field wake contracts to an area one-half that of the wing disc.

In the vortex ring approach we allow for the unsteadiness of wake generation by decomposing the cylindrical vortex sheet bounding the hypothetical momentum jet into a stack of small-cored circular vortex rings, each produced by a single wingbeat. Therefore T_w is the time for which a single vortex ring must support the bird; it is from this that ring circulation is determined.

Since the limiting equilibrium state for a wake composed of circular coaxial rings interacting with one another is unknown we analyse the fluid motion starting from rest, in the absence of any vorticity, with the wing motions being assumed to release rings at equal time intervals T_w. Induced power is given by the limiting value of the rate of energy increment as time progresses. Although the analysis involves some complexities the induced power approaches a definite limiting value. For details of the calculation see Rayner (1979*a*).

The other important parameter describing the wake evolution is the non-dimensional radius of each ring when released, R'; all linear dimensions can be expressed in terms of the initial radius which is $R'b$. The radius will be less than the semi-span, so that $R' < 1$, because of momentum balance. The value of R' is found by equating the momentum of the vortex ring to the momentum of the vortex sheet shed by the wings. Suitable values are

$$R'^2 = 0{\cdot}923\phi/\pi \tag{10}$$

in normal hovering, and

$$R'^2 = 0{\cdot}808\phi/\pi \tag{11}$$

in avian hovering, where stroke amplitude ϕ is in radians; typically ϕ is between $\frac{2}{3}\pi$ and π.

The limiting value assumed by the induced power as calculated by this model corresponds closely to the formula

$$P_i = P_{i,M}/R' \tag{12}$$

in normal hovering (in all such cases f is small, approximately in the range 0·005–0·015), and to

$$P_i = \left(\frac{0{\cdot}95}{R'} + \frac{1{\cdot}2f}{R'^5}\right) P_{i,M} \tag{13}$$

in avian hovering. When f is larger than about 0·05 with $\phi = \pi$, or for any f if ϕ is small, the momentum jet estimate $P_{i,M}$ is significantly too low, and as f increases the inaccuracy becomes greater.

This conclusion agrees with what we know of the behaviour of the flow geometry. When f is small the rings are close together; there can be little fluid flow through the wake boundary, and the situation is close to the momentum jet generated by an actuator disc of radius $R'b$ (the initial ring radius). Note that the radius of this disc is smaller than the radius of the wing disc, which was used in deriving $P_{i,M}$. If b is

replaced by $R'b$ in (8), we see that the induced power required to sustain this narrower momentum jet is greater than $P_{i,M}$ by a factor R'^{-1}, and is identical to the estimated induced power P_i (12). We can conclude that tip losses are negligible in normal hovering and that the momentum jet is a good model for power consumption. For reasons which are explained in Rayner (1979*a*, section 6), it is not a good description of the *shape* of the wake.

For larger values of f the rings are further apart; fluid can flow through the wake boundary so that we can no longer apply the conditions of mass and momentum conservation, and also work is done accelerating fluid particles outside the wake. Equation (13) gives a good estimate of the tip losses associated with avian hovering; they are an important constraint on hovering proficiency for the larger insects and the birds. Sample values of P_i are given in Table 3(*a*) and (*b*).

It is a familiar result (Lighthill, 1977) that the scaling of $P_{i,M}$ is unfavourable to larger animals; this has been used to suggest why sustained hovering is rare in animals over 20 g in mass. Equation (13) indicates that this scaling effect is even worse, for increase of tip losses with size is significant in the range of masses of large insects and small birds.

Apart from the theoretical merit that the vortex ring theory gives a better fluid dynamical description of the wake than the momentum jet, there is some experimental evidence for the rings' presence. Magnan, Perrilliat-Botonet & Girard (1938) obtained photographs of vortex rings beneath a pigeon in slow flight, and Ellington (1978) photographed them beneath a tethered hovering insect. Both of these observations also reflect an additional property of the model. At the lower end of the wake adjacent vortex rings coalesce to form a single ring of large core radius, which grows and then breaks away, leaving another to be formed in its place (see Fig. 3); it is these large rings which Magnan and Ellington have photographed.

To obtain the least possible induced power an insect or bird of fixed morphology (fixed f and $P_{i,M}$) need only increase stroke amplitude ϕ (or modify wing circulation distribution) to obtain the maximum possible ring radius R'. This also has the effect of reducing the required lift coefficient, but increases the profile power. For the smallest insect induced power is relatively low, and the main component of power consumption is the profile power. As size increases the balance alters; for the smaller birds profile power in hovering is small and it is induced power that is dominant. Larger birds (and many of the smallest) are often unable to provide sufficient power output for hovering. These considerations are discussed in detail by Weis-Fogh (1977).

The balance between induced and profile powers, together with structural limitations on size of stroke amplitude, leads to a scale-dependent optimum value of ϕ which is presumably adopted by most animals. Provided that all values of ϕ can be reached, we would expect the smallest insects to use a small ϕ, with larger insects choosing a larger value; there are however so many factors in play that it would be difficult to claim this as little more than a general rule.

In the case of the birds (f between 0·03 and 0·20) the only significant component of hovering power is induced. Few birds are capable of sustained hovering, but many can make a few strokes when landing or taking off; in these cases muscular contraction is probably anaerobic. Weis-Fogh & Alexander (1977) have estimated that the

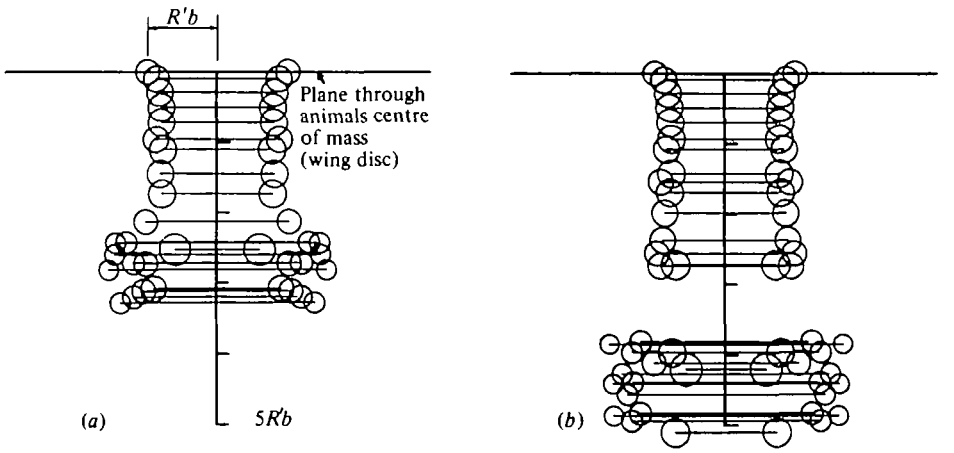

Fig. 3. Diagrammatic cross-section through hovering vortex ring wake for small insect (e.g. *Tipula* or *Eristalis*) with $f = 0{\cdot}005$. Circles represent vortex cores; larger radius rings have smaller cores. Note the smooth boundary of the stack of rings just below the wing disc. At this (low) value of f, rings are close enough together for inflow through the boundary to be small, so that the areal contraction is only slightly greater than one half. In (*a*) 21 rings are present and a bound vortex is being formed at the lower end of the stack of rings. In (*b*) 29 rings are present and the bound vortex formed of the oldest 14 rings has broken away from the stack and no longer influences the flow around the wing disc.

absolute maximum continuous power output from striated muscle is about 250 W per kg muscle mass; as a conservative estimate we may assume a bird can obtain 80% of this, giving available power P_a of $200 \times \frac{1}{8} m_p$ W, where m_p is the pectoral muscle mass in kg; the factor of $\frac{1}{8}$ represents the approximate proportion of the total stroke which is powered. Values of P_a are compared with the aerodynamic power P_i in Table 3(*b*); estimated P_a for larger birds is likely to be inaccurate because it is unlikely that they could obtain as much power; the quoted values of P_a will be too great. The pied flycatcher is known to hover above its nest (Norberg, 1975) with $\phi = 100°$; it is not clear whether this observation was of sustained hovering, but it is more likely not. P_i needed at this stroke amplitude is 0·23 W, compared with P_a of 0·19 W; we deduce that muscle contraction is probably anaerobic and hovering was not sustained. However, the flycatcher may possibly be capable of sustained hovering with a larger stroke amplitude. Evidently the wren, kestrel, mallard and pheasant have insufficient power to hover (although the pheasant can take off almost vertically when flushed), but with a large stroke amplitude the pigeon would probably not incur a significant oxygen debt. Pigeons taking off can be observed to clap their wings dorsally (ϕ almost 180°) and probably generate wing circulation by a 'fling'. The tern (which has an unusually low value of f) and the long-eared bat (cf. Norberg, 1976*b*) should be fully capable of sustaining hovering flight.

We can give no support to the suggestion that kestrels hover before swooping onto their prey. Their available muscle power is considerably lower than they would require even for anaerobic hovering, The observations must be explained by flight into a low-velocity wind; power consumption would be much lower than in hovering, and stability and position-fixing ability would be greatly improved.

Table 3. (*a*) *Induced power in normal hovering*

(This table only quotes power consumption $P_{i,M}$; that is, the momentum jet estimate. P_i is obtained by multiplying $P_{i,M}$ by a simple conversion factor: 1·04 when $\phi = 180°$ and 1·47 when $\phi = 90°$.)

	Mass, M (kg)	Momentum jet induced power, $P_{i,M}$ (W)	Specific m.j. induced power $P^*_{i,M}$ (W kg^{-1})
*Encarsia formosa**	$2{\cdot}5 \times 10^{-8}$	$6{\cdot}3 \times 10^{-8}$	2·5
Drosophilia virilis	2×10^{-6}	$1{\cdot}0 \times 10^{-5}$	5·2
Tipula paludosa	$2{\cdot}8 \times 10^{-5}$	$9{\cdot}5 \times 10^{-5}$	3·4
Eristalis tenax	$1{\cdot}5 \times 10^{-4}$	$1{\cdot}6 \times 10^{-3}$	10·7
Bombus terrestris	$8{\cdot}8 \times 10^{-4}$	$1{\cdot}7 \times 10^{-3}$	19·0
Manduca sexta	$1{\cdot}12 \times 10^{-3}$	$8{\cdot}3 \times 10^{-3}$	7·4
Amazilia fimbriata	$5{\cdot}1 \times 10^{-3}$	$6{\cdot}9 \times 10^{-3}$	13·4
Patagona gigas	0·02	0·24	12·1

* Reynolds number too small for vortex theory to be appropriate.

Table 3. (*b*) *Induced power in avian hovering*

	Mass, M (kg)	Available power, P_a (W)	Induced power requirement, P_i (W)			
			$\phi = 90°$	$\phi = 120°$	$\phi = 150°$	$\phi = 180°$
Wren	0·010	0·12	0·46	0·30	0·23	0·19
Flycatcher	0·012	0·19	0·25	0·20	0·17	0·15
Tern	0·118	1·9	2·0	1·6	1·4	1·2
Kestrel	0·245	2·9	7·8	5·9	4·9	4·3
Pigeon	0·333	6·4	17·6	12·4	9·9	8·5
Mallard	1·105	21	69	50	40	35
Pheasant	1·660	32	179	119	91	76
Long-eared bat	0·009	0·13	0·11	0·09	0·08	0·07

In Table 3(*a*) we see values of $P_{i,M}$ and specific momentum jet power

$$P^*_{i,M} = P_{i,M}/M \quad \text{(W per kg body mass)}$$

for six insects and two hummingbirds. The chalcid wasp *Encarsia* is probably too small for the vortex theory to be appropriate as viscous forces are significant. Of the other insects, the crane-fly *Tipula* and the moth *Manduca* both have abnormally large wing spans, and therefore relatively low specific induced powers. On the other hand, the bee *Bombus* has very small wings (its mass is 30 times that of *Tipula*, yet the wing span is the same) and induced power is very high, quite possibly too high for sustained hovering. The larger hummingbird *Patagona* is near to the maximum size at which hovering flight is possible; it is only able to sustain hovering by having a large (25 cm) wing span and pectoral muscles comprising 30% of its total mass (Lighthill, 1977).

The optimum strategy for a bird or insect intending to hover or fly slowly is to maximize R' by increasing the stroke amplitude and controlling wing circulation, and to minimize f by reducing stroke period. This strategy reduces both induced power and the required lift coefficient, but for the smaller size range can bring a significant rise in profile or inertial power. The main morphological features we expect to see in hovering animals are a low disc loading (large wing span) and the capacity for large fast wing strokes (large ϕ and small T). Towards the upper range of masses we also expect, as typified by the hummingbirds, proportionately large flight muscles. It must

also be remembered that over-specialization for slow or hovering flight often results in highly inefficient fast flight.

We have seen that the wake in hovering flight is composed of a chain of vortex rings, but have not discussed the mechanism by which they are generated. This topic is considered in the context of forward flight in section 3; the ideas given there may be extended readily to hovering.

3. AVIAN FORWARD FLIGHT

The use of the vortex ring theory to describe avian forward flight is similar to the approach to avian hovering, but is complicated by the requirement that the momentum of each vortex ring must balance parasite and profile drags in addition to the bird's weight. The ring is not circular, and is inclined to the horizontal. It is important that the upstroke performs no useful aerodynamic function, so that we may assume that the vortex elements shed by each downstroke are distinct; they are separated from each other both by the motion of the bird and by their own convection. This assumption is satisfactory in most cases of forward flight (Brown, 1963; Norberg, 1975, 1976*a*), but in fast forward flight some large birds do use their upstroke for lift generation, and we must exclude this case. For the same reason we do not discuss forward insect flight.

The main fact distinguishing natural from mechanical flight is that the same pair of organs, the wings, must produce lift and thrust, and that therefore the vortex wake shed by the wings must balance weight and drag together (including, paradoxically, the extra drag incurred in wake generation). A slightly similar situation occurs in helicopters, but cannot be related to avian flight because of a bird's reciprocating wings; although it is frequently used elsewhere the analogy is not helpful.

The simplest method of deriving induced power in forward flight would seem to be calculation of the mean rate of working against induced drag by the wing sections. This would be possible if we knew induced drag coefficients at all times during the stroke for the whole wing span. However, as we have seen, it is not possible to estimate these coefficients because of the unsteady airflow around the wing disc, and calculations based on steady state values for suitable wings are unlikely to be useful. In fact, the simplest way of estimating the lift and induced drag coefficients is probably the reverse of this procedure, involving a balance of the forces acting (Norberg, 1976*a*). A more complicated approach using lifting surface theory gives sensible, if laborious, results (Hummel & Möllenstädt, 1977).

The only previous power model taking account of stroke kinematics is that of Pennycuick (1968, 1969, 1975), with related versions modified to agree with experimental observations (Tucker, 1973, 1977). Pennycuick derives induced power from momentum jet theory, having invoked the helicopter analogy. This approach gives sensible results, but for a number of reasons is not satisfactory, Firstly, as in hovering, wake generation is not steady. Secondly, momentum jet theory does not allow for down-wind convection of the far field wake due to the bird's forward velocity, while thirdly, and of greatest significance, there is no obvious way of defining the actuator disc (necessary for wake generation) in terms of the geometry of the downstroke. In a momentum jet, wake momentum must be perpendicular to the actuator disc and parallel to the wake axis; when wake generation is not steady it is not possible to satisfy this condition (see Fig. 4).

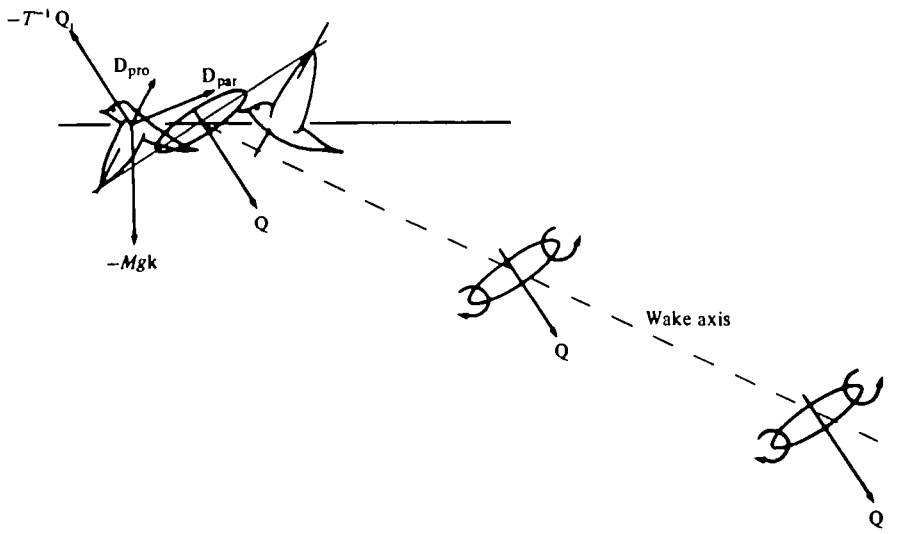

Fig. 4. Diagram of vortex wake in avian forward flight, showing the forces acting on the bird. The lifting and sustaining force $-T^{-1}\mathbf{Q}$ is the mean reaction of vortex ring momentum $\mathbf{Q}$ for time T. The profile drag $\mathbf{D}_{pro}$ and parasite drag $\mathbf{D}_{par}$ also have some lifting effect. Note that the wake momentum is not parallel to the wake axis.

A more satisfactory form of the wake which does not violate the conditions above is a chain of vortex rings of suitable shape, position and momentum. We cannot assume that these rings are circular, but take them to be ellipses elongated from circles in the direction of flight. This assumption about the shape of the rings is difficult to justify theoretically, and the true shape needs to be found experimentally. Some simplifying assumption of this kind is needed to make numerical calculations possible, and this shape agrees well with downstroke geometry (see Rayner 1979*b*, section 3). The proportions of the ring are determined from stroke kinematics, the size from wing circulation distribution.

The trailing vorticity shed by the wings occupies initially a complex twisted surface with both streamwise and transverse vorticity (see Fig. 5*a*); only in hovering is this sheet planar and of simple (circular) geometry. Because of the immensity of the numerical calculations involved we cannot trace the evolution of this sheet, but by analogy with the known properties of the wake of a rigid straight wing we hypothesize that it will roll up into a region of concentrated vorticity, a small-cored vortex loop. In addition, there is the evidence of Magnan *et al.* (1938), in which vortex rings were observed behind a pigeon in slow flight.

It must be emphasized that we are concerned here with steady level flight in near ground level atmospheric conditions. Accelerating or climbing flight entails a modification of the force balance on the animal and is not discussed.

The arguments for the determination of vortex ring size, strength and geometry are complicated and cannot readily be simplified. They are set out in detail in Rayner (1979*b*), sections 3 and 4, and are briefly repeated here. The forces on a bird in steady flight consist of its weight, body parasite drag (dependent on mass M and stroke plane angle γ), wing profile drag (calculated from morphological and kinematic parameters) and the total induced forces; these all must be in equilibrium (Fig. 4).

The induced forces must be the reaction of the mean force provided by a single vortex ring. The two components (forward and vertical) of the balance of forces allow exact determination of ring circulation and stroke plane angle γ at all flight speeds, for realistic values of the remaining kinematic parameters T (stroke period), τ (downstroke ratio) and ϕ (stroke amplitude). Any inertial forces acting on the body do some (small) work but have no mean reaction. They do not need to be included in the force balance because they average to zero over a whole stroke; Weis-Fogh's (1977) calculations of scaling indicate that in the size range of birds inertial work rate is negligible. We neglect recoil of the bird's body since this is observed to be small (e.g. Pennycuick, 1968).

Induced power P_i is calculated, as in hovering, from the kinetic energy increment in the wake in a single stroke. This increment has two components: one is the self-energy of the newly generated ring, the other the mutual (interactive) energy of the new ring with each of the existing rings in the wake. In hovering, mutual energy dominates and is calculated by the method described in section 2. As flight velocity increases, mutual energy falls rapidly and above the minimum power speed is negligible. We need not consider in detail the configuration of the far field wake; an approximate description is adequate at medium velocities where only the immediately generated ring is of any significance. At high velocities the elliptical ring is highly eccentric and distorts (and probably annihilates itself) very rapidly; this problem cannot affect the power estimates made by the model.

Estimation of profile and parasite powers is less complicated. Following Rayner (1979*b*), equation (37), we find profile power at flight speed V to be

$$P_{\text{pro}} = \tfrac{1}{T}\mu\rho bc_0\int_0^1 \bar{c}(\zeta)\left\{\int_0^{\tau T}(V^2+2Vb\zeta\dot{\theta}\cos\theta\cos\gamma+b^2\zeta^2\dot{\theta}^2)^{\frac{3}{2}}C_D(\zeta,t)\,dt\right\}d\zeta, \quad (14)$$

where θ is the angular position of the wing during the downstroke; if assumed sinusoidal, this is

$$\theta(t) = -\tfrac{1}{2}\phi\cos(\pi t/\tau T); \quad (15)$$

$C_D(\zeta, t)$ is the local profile drag coefficient.

The muscle ratio $\mu = (m_s+m_p)/m_p$ is introduced to take account of the small amount of work done against profile forces on the upstroke; we already know that no induced forces act. Although rather arbitrary, the correction is small; in general, $\mu \approx 1{\cdot}15$. The double integral in (14) is similar to those found by Osborne (1951); Osborne found no simple analytic solution (correctly, for none exists) and introduced various approximations. With numerical computation the exact evaluation of (14) is straightforward, to obtain $P_{\text{pro}}(V)$ when τ, T and ϕ are determined. The only uncertainty in (14) is the value assigned to the profile drag coefficient $C_D(\zeta, t)$. This is the zero lift drag coefficient for the wing, and there is very little data available. We take a constant value $C_{D0} = 0{\cdot}02$, around the higher values found in aeronautics, although much higher values are likely in small insects (Vogel, 1967). Bird wings are highly efficient aerofoils, and deform automatically to the optimum (minimum drag) shape. In view of this deformation it is not easy to define 'zero lift' drag exactly, since at no angle of incidence can there be no induced drag. The bird has great control over the airflow past its wings; such devices as the alula and primary feather separation

can limit the onset of turbulence or of flow separation, and the downy covert feathers just behind the leading edge on both sides of the wing help drag reduction by keeping flow laminar, in much the same way as the skins of cetacean mammals. With all this in mind a value for C_{D0} of 0·02 appears realistic; other values of the same magnitude would alter power consumption at high velocities, but not the relative effects of the variations in stroke parameters considered in section 4.

Parasite power P_{par} is given by the formula

$$P_{\mathrm{par}} = -\mathbf{D}_{\mathrm{par}} . V\mathbf{i}, \tag{16}$$

where $\mathbf{D}_{\mathrm{par}}$ is the total parasite drag of the body, used in the force balance described above. Any lift (and associated induced drag) generated by, for instance, tail or feet should be included in (16). The difficulties arise from determining $\mathbf{D}_{\mathrm{par}}$ for different flight speeds. There is a great lack of accurate information and a need for a wide-ranging set of experiments to determine it. It is virtually impossible to predict $\mathbf{D}_{\mathrm{par}}$ (even neglecting the effects of tail and feet) from the few available data. However, accurate experimental measurements of this kind on wingless carcasses are very hard to make; for a number of reasons many of those which have been made cannot be relied upon. The author's own efforts in this direction failed to give more than an indication of the orders of magnitude of the forces involved (fortunately confirming the crude estimates used below).

There are a number of possible representations for $\mathbf{D}_{\mathrm{par}}$, which are discussed in detail in Rayner (1979*b*). In all cases it is assumed to be of the form

$$\mathbf{D}_{\mathrm{par}} = \tfrac{1}{2}\rho M^{\frac{2}{3}}(-C_{Di}\,\mathbf{i} + C_{Dk}\mathbf{k})\,V^2, \tag{17}$$

where C_{Di}, C_{Dk} are drag coefficients, possibly depending on the angle β at which the body is tilted but otherwise constant. The term V^2 is usual for drag representations in the appropriate range of Reynolds numbers; moreover this range for birds (not insects) is close to that for which a sphere's drag coefficient remains constant, so we may assume (13) to be suitable for all birds at all speeds. Although some authors have attempted to include Reynolds number effects (Tucker, 1973; Greenewalt, 1975; Pennycuick, 1975), any increased accuracy (assuming no inaccuracy is introduced) would be offset by the large inaccuracies in available data. The term in $M^{\frac{2}{3}}$ gives some indication of the behaviour of $\mathbf{D}_{\mathrm{par}}$ as size varies; the index derives from isometric scaling (see section 4). In the absence of thorough measurements we must allow it to stand; it is confirmed by some measurements of Tucker (1973).

The simplest form for parasite drag is that used by Pennycuick (1968). Assuming that the body remains untilted ($\beta = 0$), and based on measurements for the pigeon,

$$C_{Di} = 2{\cdot}85 \times 10^{-3}, \tag{18}$$

and $C_{Dk} = 0$. Tucker (1973) found the slightly greater horizontal drag component

$$C_{Di} = 3{\cdot}34 \times 10^{-3}. \tag{19}$$

Since Tucker's value was derived from measurements of seven different species it is more likely to be reliable. If now we model the results of tilting the body by the form for the drag of a tilted circular cylinder, we obtain

$$\left.\begin{aligned} C_{Di} &= C_{D1}\cos^3\beta + C_{D2}\sin^3\beta, \\ C_{Dk} &= (C_{D2}\sin\beta - C_{D1}\cos\beta)\sin\beta\cos\beta, \end{aligned}\right\} \tag{20}$$

where C_{D1} takes one of the values of (18) or (19), and C_{D2} is unknown. Morphological measurements by the author on a pigeon suggest $C_{D2} = 4{\cdot}5 \times 10^{-2}$; the order of magnitude would be expected, but it can hardly be claimed that a pigeon alone can give sufficiently accurate estimates for other birds.

The only measurements of the effect of body tilting were made by Csicsáky (1977), using plaster models of the zebra finch. Recalculated in the form of (17) these give

$$\left.\begin{aligned} C_{Di} &= \{1{\cdot}142 + 7{\cdot}141\,(\beta - \tfrac{1}{36}\pi)^{2{\cdot}434}\} \times 10^{-3}, \\ C_{Dk} &= 7{\cdot}486\,(\beta - \tfrac{1}{36}\pi)^{1{\cdot}405} \times 10^{-3}, \end{aligned}\right\} \tag{21}$$

where β is in radians. These have similar behaviour as functions of β to the form of (20) but are in magnitude between $\frac{1}{2}$ and $\frac{1}{3}$ of that estimate; the discrepancy is probably explained in part by the use of models and in part by the small size of the samples used in both cases.

We must also discuss the relation between β and the other kinematic parameters, in particular the stroke plane angle γ; this depends on the degree of articulation assumed at the humeral joint, no doubt significantly dependent on species. Total rigidity would suggest, say,

$$\beta = \tfrac{8}{9}\pi - \gamma, \tag{22}$$

while with a larger amount of freedom

$$\beta = \max(\beta_1 - \gamma, 0), \tag{23}$$

where β_1 may lie between about 35° and 80°. Again, more research is needed to clarify this point; for the finch, Csicsáky quotes $\beta_1 = 55°$. Rayner (1979*b*) discusses the effect of experimenting with the $\beta(\gamma)$ relation and with the values of C_{Di} and C_{Dk}.

Both parasite and profile powers increase with V (for large V, as V^3) and are of comparable magnitude. Induced power falls rapidly from a high value when $V = 0$, decaying approximately as V^{-1} for large V. The total aerodynamic power as a function of velocity is a U-shaped curve, with a definite speed V_0 at which power is minimized and a higher speed V_1 at which cost of transport $C(V) = P(V)/Mg\,V$ is minimized.

It is common (e.g. Tucker, 1973) to compare this curve with independent measurements of chemical (physiological) power consumption to determine the bird's efficiency of energy conversion or, more usually, to refine the aerodynamic model. In view of the several uncertainties involved, this should not be encouraged until we have a much greater understanding of a bird's muscular physiology. In particular, the muscular efficiency almost certainly depends on the muscle contraction length and rate, and hence depends on kinematic parameters, which for any individual depend on flight speed. Thus, efficiency varies with speed in an effectively unpredictable way. For similar reasons, we do not attempt to deduce maximum continuous (or burst) flight speeds from the power economy.

It remains to consider the mechanism for the generation of the vortex rings; although not important to the power calculation the topic is at the heart of most natural flight mechanisms. Very little is known about the air flow around the wing

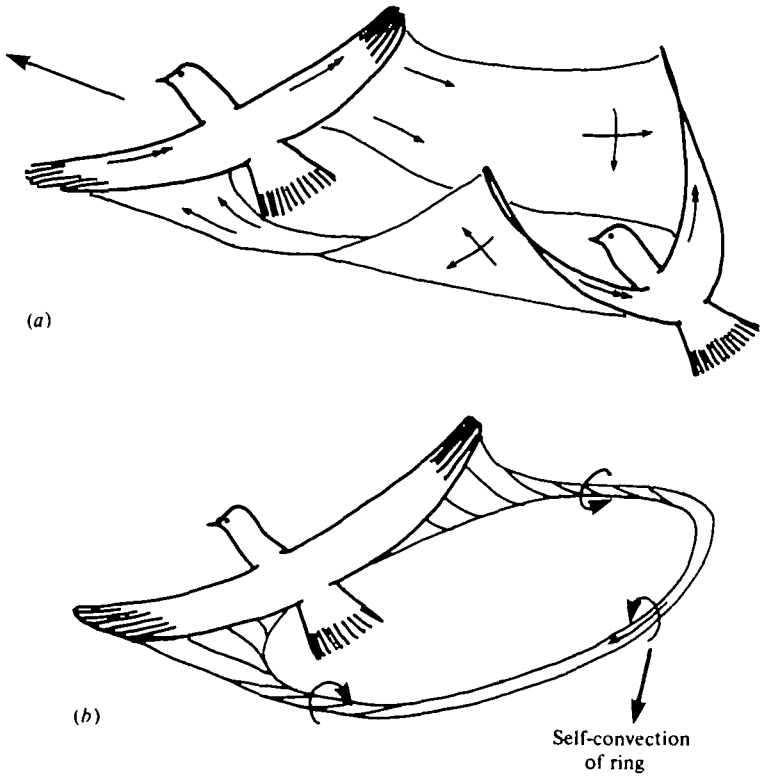

Fig. 5. (*a*) The first half of a bird's downstroke in forward flight, showing the surface which comprises the loci of points on the wings. These are also the loci of points occupied by trailing vorticity immediately after being shed. The surface would also be the shed vortex sheet if this did not deform. Single arrows indicate the sense of the vorticity present in different portions of the sheet, and double arrows represent the sense of the bound vorticity on the wings. (*b*) The supposed distribution of wake vorticity during a downstroke, at the same instant as (*a*), showing how the trailing vortex sheet has rolled-up into a portion of a vortex ring. This ring convects downwards under its self-induced motion.

and we can do little more than speculate about what occurs. The explanation below should be read in conjunction with Fig. 5(*a*) and (*b*), since a purely verbal description of the shape of the vortex distribution in three dimensions is doomed to failure!

Whenever a lift-generating rigid wing moves steadily relative to the air surrounding it, the effect on the air may be likened to that of a bound line vortex on the leading edge combined with the appropriate translation. At the wingtips the discrepancy in pressure between the two surfaces of the wing encourages leakage of air around the tips from bottom to top; near the tip, therefore, the airflow over the upper surface is deflected inwards and that past the lower surface outwards. Since vortex lines are always closed, the bound vortex on the wing must be part of a loop, the other parts of which are two trailing vortices and a starting vortex at the place where the wing first started to move. These flows can often persist stably for a considerable time before the effects of viscous dissipation are apparent.

If circulation (strength of the bound vortex) is not constant across the span a trailing vortex sheet is left behind the wing, with varying circulation density; further,

when the wing accelerates or decelerates transverse vorticity is also shed. There is a considerable body of experimental and theoretical evidence that the sheet behind a rigid wing in steady level flight rolls up into a pair of concentrated vortices, within a short distance (about 2 chord lenths) of the wing. The separation of the pair is found by momentum conservation, the core radius by energy conservation. The rate of change of vertical momentum of the vortex distribution in the wake is exactly adequate to balance other vertical forces acting on the aircraft (mainly weight); horizontal momentum change causes induced drag, which must be countered by engine thrust. Induced power is usually found as the rate of working against induced drag forces, but can also be calculated (to give an identical result) as the rate of change of wake kinetic energy.

The above procedure is familiar from classical aerodynamics, and is explained in greater detail in any textbook on the subject. The situation in animal flight is related to this, but as we have already seen the unsteady flow causes problems if induced drag is considered. An animal must contrive its wingbeat to generate some forward component of momentum, since it cannot resort to engine thrust to overcome drag. The induced drag on the wings always points backwards; the wingbeat must therefore be both forward and downwards, so that sectional lift can give some thrust to the body. For these reasons it is not helpful to discuss the different portions of the wing as having different functions; all contribute to the single lift and thrust generating vortex ring.

The trailing vortex sheet for the first part of the bird's downstroke is shown in Fig. 5(*a*). The arrows indicate the vector direction of vorticity locally in the wake. It must be emphasized that the sheet as drawn represents the locus of wing positions during the downstroke, and is merely the *intial* position of each vortex element. The wing shape shown at the start of the downstroke has bound vorticity of the *opposite sense* to that left in the wake as the starting vortex as the wing moves forward from this position.

By analogy with the planar vortex sheet of an aircraft a small-cored vortex ring will be formed; Fig. 5(*b*) shows a realistic configuration for the vorticity in the wake at the middle of the downstroke. The outward and downward twist in the vortex sheet matching the wings' motion are in the correct sense to assist and encourage roll-up, which is a result of mutual interaction of the vortex elements forming the sheet. At the end of the downstroke a sudden vertical acceleration of the wings results in a closing vortex line which completes the loop. The shape of the elliptical vortex loop is determined by stroke geometry, the size by momentum equality with the vortex sheet. Non-dimensional core radius is estimated as 0·171, that found behind an elliptically loaded straight wing. Since the 'oldest' (first generated) part of the ring is curved it convects downwards; the magnitude of the convection velocity is suitable to need a tilted stroke plane of up to 30° in hovering, as observed, if wake momentum is to be vertical; in forward flight circulation is much lower and convection is less important.

Some recent research into wing tip 'sails' on aircraft (Spillman, 1979), which are rather similar to separated primary feathers, suggests that feather separation has the effect of widening the region occupied by the vortex sheet. If this is indeed the case a bird would appear to be operating as if with a greater aerodynamic wing span than the limitations on structure might permit, with a corresponding reduction in both lift coefficient and induced drag.

All of the above discussion applies equally to hovering of birds and insects; Fig. 5(*a*) and (*b*) is still appropriate if no forward velocity is present. In normal hovering the rapid flick of the wing at the end of each portion of the stroke serves to 'shake off' any remaining bound vorticity.

4. POWER CONSUMPTION AND FLIGHT STYLE

As flight velocity increases, induced power falls and parasite and profile powers rise, resulting in a U-shaped curve of total aerodynamic power P against velocity V. Sample power curves for five representative species (wren, *Troglodytes troglodytes*; pied flycatcher, *Ficedula hypoleuca*; pigeon, *Columba livia*; mallard, *Anas platyrhynchos*; pheasant, *Phasianus colchicus*) are shown in Figs. 6–8; data for these birds are given in Table 2(*b*). All calculations discussed are performed with the drag representation given by (17), (19) and (20), with stroke amplitude $\phi = 120°$ and downstroke ratio $\tau = \frac{3}{7}$.

The power curve defines two characteristic velocities: V_0 at which total power $P(V)$ is minimized [$P(V_0) = P_0$], and V_1 at which cost of transport $C(V)$ is minimized [$C(V_1) = C_1$]. V_1 is greater than V_0. In most cases the minimum is very shallow and there is little increase in power or cost with a moderate change in velocity. The hovering induced power is calculated from (13), being more accurate at low speeds than the limiting form of the forward-flight model; where appropriate the low speed values of power are interpolated by eye and are indicated in Figs. 6, 7 and 9 by dashed lines; they are omitted for the mallard and the pheasant, since these species are too large to be able to hover.

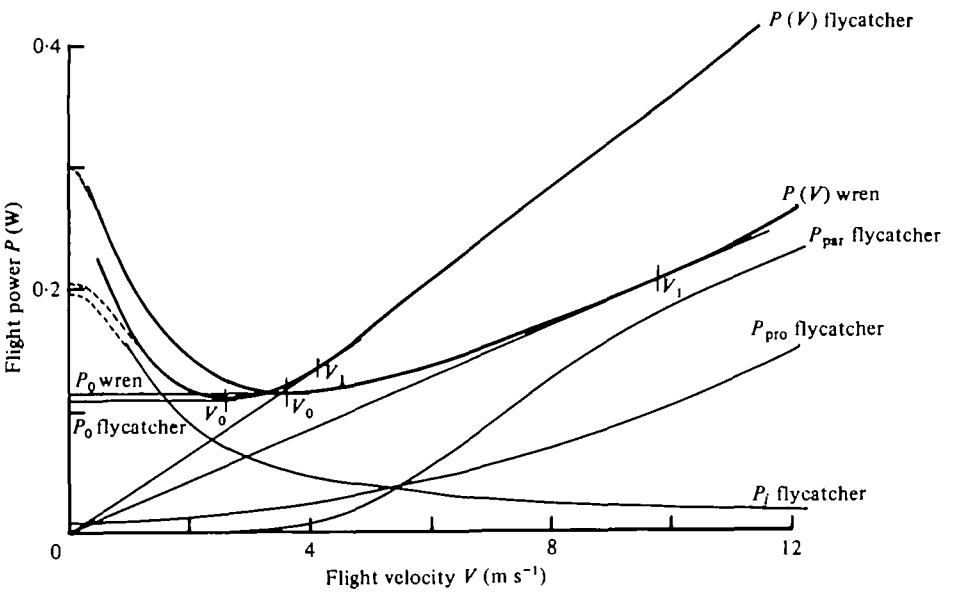

Fig. 6. Power curves for wren (mass 0·010 kg) and flycatcher (0·012 kg). For details of calculation see text. Dashed portion of curves at low velocities are interpolations from exact induced power in hovering, as calculated in section 2. Note the high parasite power for the flycatcher, and associated low minimum power speed V_0. High cost of transport for this bird results from high profile power, but is not actual cost of forward flight since bounding flight is used.

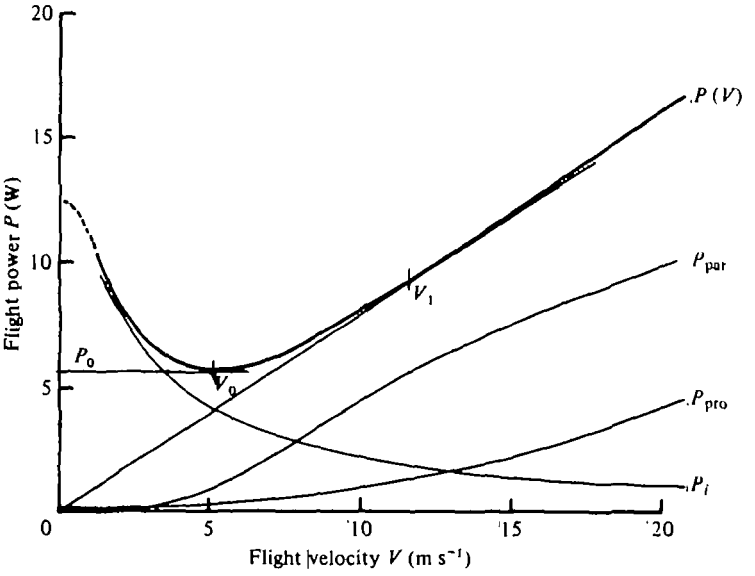

Fig. 7. Power curves for pigeon (mass 0·333 kg). Note the high minimum cost speed V_1.

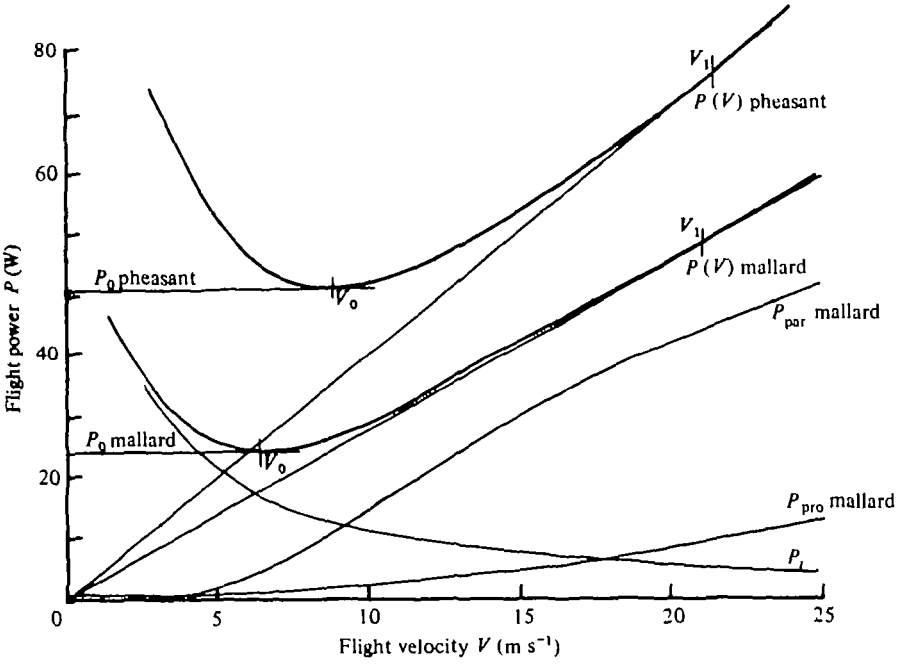

Fig. 8. Power curves for mallard (1·105 kg) and pheasant (1·66 kg). Note relatively high minimum cost speed for both birds and relatively high power at all speeds for pheasant. The small wings of the duck result in low profile power, and slow increase in power with speed.

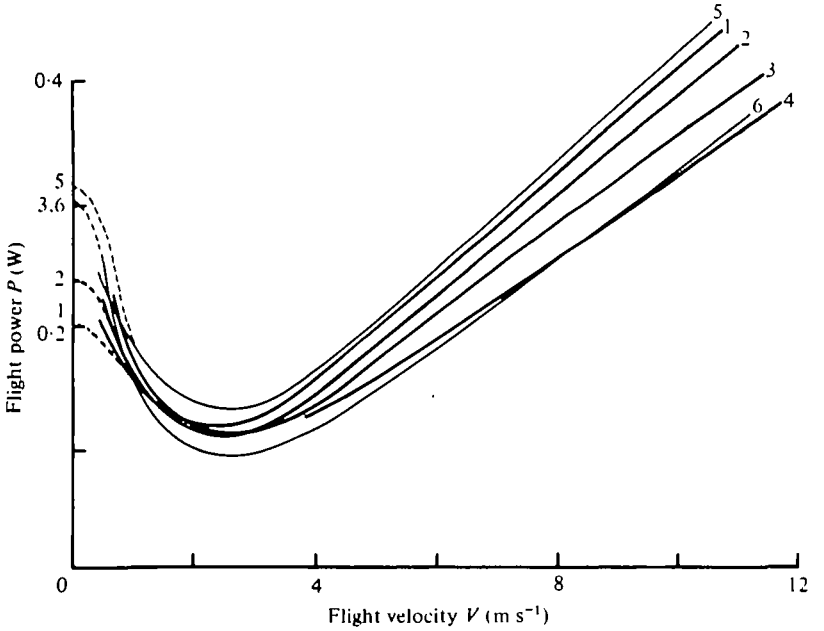

Fig. 9. Comparison of effect on power consumption of varying kinematic parameters ϕ (stroke amplitude) and τ (downstroke ratio) assuming that other parameters remain constant, for flycatcher. (1) $\phi = 180°$, $\tau = \frac{1}{2}$. (2) $\phi = 150°$, $\tau = \frac{1}{2}$. (3) $\phi = 120°$, $\tau = \frac{1}{2}$. (4) $\phi = 90°$, $\tau = \frac{1}{2}$ (not illustrated for small V). (5) $\phi = 120°$, $\tau = \frac{1}{3}$. (6) $\phi = 120°$, $\tau = \frac{2}{3}$.

Cost of transport, defined as

$$C(V) = P(V)/Mg(V), \tag{24}$$

measures the aerodynamic work done by the bird transporting unit weight through unit distance; it is a non-dimensional quantity. The bird will choose to fly at the minimum cost speed V_1 if it must cover a great distance, since at this speed the total energy required is least although the power required is above the minimum. The bird will select this speed provided that the rate of working then required is not greater than the maximum available from the muscles. In other conditions, particularly for short flights, the bird is more likely to select the minimum power speed V_0.

While the two speeds V_0 and V_1 characterize the power curves, they are not necessarily the speeds which minimize the cost to the fuel reserves per unit time or per unit distance. V_1 varies if there is either a head or tail wind: this calculation is concerned with flight relative to still air, and cost of transport is only useful when considered as energy per unit ground distance; in addition V_1 will increase if we include a fixed basal metabolism to account for energy consumed by body functions independent of flight. Finally, both V_0 and V_1 might alter if we could calculate the actual cost to the bird for a particular flight strategy; aerodynamic power is converted to the rate of consumption of fuel through division by muscular efficiency, which will depend upon the kinematic parameters, and hence upon flight velocity. Very little is known about the detailed dependence of this efficiency on these parameters, and we have little more than approximate estimates of its magnitude. Until we know more

about it, it is not easy to relate aerodynamic power consumption to the true rate of working, or to define exactly the speeds at which power and cost are minimized.

The stroke plane angle γ predicted by the model is generally too small in hovering and slow flight, especially for birds with low f. Predictions for the flycatcher in hovering are low by a factor of approximately 2·5; as V increases, γ rises and reaches realistic values at around the minimum cost speed. The discrepancy is caused by the lack of an accurate formula for the convective velocity of the vortex rings; the estimate we use neglects the effect of vorticity elsewhere in the wake and therefore is too low. When f is small, older wake elements are close to the bird in forward flight, and so the underestimate is greater. In fast forward flight, predicted γ is wholly realistic (in the range 60–75°). The tolerance of $\gamma(V)$ to such factors as the drag representation is slight. Although $\gamma(V)$ is inaccurate at slow speeds, the inaccuracy does not materially affect the total power consumption calculated. By modifying the convective velocity it can be shown that the power consumption is very insensitive to the values of γ, and therefore we ignore the problem.

The most important deductions from the model are those concerning flight style, as dictated by a choice of kinematic parameters. It was a feature of the model that the morphological parameters M, b, c_0 and S are assumed to remain the same at all speeds; this is equivalent to stating that the wings are not flexed at higher speeds, but have the same planform throughout the downstroke at all velocities. We assume that stroke period T is likely to be constant for any individual; stroke plane angle γ is determined by the momentum balance in the model, and in any case does not affect power consumption. The only parameters which we are able to vary are therefore stroke amplitude ϕ and downstroke ratio τ.

Stroke parameters ϕ and τ will both be limited in some way by the properties of the main flight muscles. There is a maximum contraction velocity, so that $\phi\tau^{-1}$ will be limited above, and this limit is likely to have a real effect at low velocities. The maximum force which the muscle can exert gives an upper limit to $\phi^2\tau^{-1}$, which can again be important in hovering. There are also upper limits to ϕ (dictated by the flexibility of the humeral joint) and to τ (dictated by the time to be spent on the upstroke). A contrary requirement is a lower limit on $\phi^2\tau^{-1}$ imposed by the need for the wings to generate sufficient force to sustain the bird. These simple arguments indicate that there is a range of values of ϕ and τ within which flight can be possible; the design criteria of the bird will include the need to make this range as wide as can possibly be consistent with the other demands made by its lifestyle.

The requirements of the model on ϕ and τ are clear (Fig. 9). In hovering, induced power dominates, and (13) shows that τ is largely irrelevant since profile power is small, but that a large value of ϕ is beneficial; large ϕ also lowers the lift coefficient required, so it is clearly important. In fast forward flight profile and parasite powers dominate; ϕ can be small and τ large, as far as consistent with the constraints above. Many large birds are able to adjust to the limit $\phi = 0$ and $\tau = 1$ which represents gliding; 'power' consumption is then measured by the rate of height loss. Thus to glide efficiently a bird requires high aspect ratio and low disc loading.

A compromise available to some species is intermittent flight (Rayner, 1977), which may take two forms. Undulating flight is a compromise between steady flapping and gliding, and is found in many large birds which cannot quite soar efficiently, or which

wish to retain height. The other is bounding flight, common among passerines up to about the size of the woodpecker ($M \approx 0{\cdot}3$ kg); the flight path appears sinusoidal when viewed from the side; it consists of a few wingstrokes followed by a period with the wings folded against the body. It is a mode of flight adopted by birds which have large profile drag and low disc loading (effectively large wings and small feathering parameter), typified by the flycatcher. Bounding flight gives a reduction in power consumption which is valuable for these birds whose flight power is generally high (compare the flycatcher and wren in Fig. 6: the flycatcher has relatively low disc loading and aspect ratio, and benefits greatly from bounding). The low aspect ratio and high parasite drag common among passerines rules out gliding, and hence undulating flight, as a realistic method of saving energy. In addition to the aerodynamic benefit, there may also be physiological advantages from bounding flight.

It is clear from Fig. 9 that somewhere around the minimum power speed V_0 the optimum values of ϕ and τ suffer a rapid change, representing the transition from slow to fast forward flight. This corresponds well with the observations on the swift (Oehme, 1968) and the gull (Tucker, 1972), where the flight style was seen to differ markedly between the two modes of flight. Observations on pied flycatcher hovering (Norberg, 1975) give values $\phi = 100°$ and $\tau = \frac{3}{7}$, While lower work rate might be achieved by a higher ϕ, presumably this violates the constraints on muscle strength; alternatively, high values of ϕ may result in abnormally low muscular efficiencies, and hence an enhanced total power consumption, making $\phi = 100°$ the optimum. Other birds have less strict constraints; for instance the pigeon can 'clap' its wings dorsally (thereby gaining from the Weis-Fogh clap-and-fling) so in hovering and slow flight can have access to values of ϕ of nearly 180°.

Fig. 9 illustrates only the effect of varying ϕ and τ for the flycatcher, but the relative shapes of the power curves for species are similar; there is always the same change in flight style at about V_0, the same preference for high ϕ in slow flight and low ϕ in fast flight, and for high τ throughout. However, as we expect, some species show a preference for slow flight, others for fast, as befits their life style, and this is reflected in the shape of the power curve. The five species serve to illustrate this well. Curves for these birds are illustrated in Figs. 6–8; all are drawn with $\phi = 120°$ and $\tau = \frac{3}{7}$.

The wren and the pied flycatcher are both small birds ($M \approx 0{\cdot}01$ kg). The wren has short, rounded wings; it uses short, relatively slow flights, and is not agile; by contrast the flycatcher (preferring open fields to the bushes and trees of the wren) has large pointed wings, is very agile, and can fly fast, often using pronounced bounding; disc loading N_d and feathering parameter f are both high for the wren and low for the flycatcher. The effect on the power curves is evident in Fig. 6. That for the wren has a much shallower minimum than the flycatcher's; hovering power is very high, but forward flight power is much lower, while the wren might fly faster than the flycatcher. However, we see from Table 1(*b*) that the muscle mass of the wren (m_p) is relatively low (among the smallest proportions of all birds) so that available flight power is strictly limited; indeed it may be that all of the wren's flights take place under anaerobic conditions. The flycatcher has more power available and by virtue of its low disc loading uses bounding flight efficiently to bring about a valuable saving in total enery cost.

The pigeon (Fig. 7) has wings of low aspect ratio, high f and high disc loading; it also has very large pectoral muscles. These combine to give it agility under all flight conditions; its ability to reach high values of ϕ avoids any difficulty in obtaining sufficient lift, while the muscles have sufficient power in reserve to allow it strong and direct fast flight. Of all species the pigeon is probably the best adapted to all flight conditions.

The two larger birds, the mallard and the pheasant, both averaging in weight over 1 kg, are well in the range where powered flight is difficult to sustain in all conditions. Birds of this size cannot hover, even for short periods, and often experience difficulty in take-off. The mallard makes a long 'pattering' run across the surface of the water in order to gain sufficient air velocity over the wings for lift-off (probably assisted by aerodynamic ground effect); in flight it has a steady powerful wingbeat and is one of the fastest of all birds. On the other hand, the pheasant can take off almost vertically when flushed, and yet prefers to run on the ground to escape predators; its forward flight is heavy and laboured, and is rarely sustained for long periods. The reason for the discrepancy between the mallard and the pheasant is their wing shape; both have relatively small wings (as is usual in large birds with a major proportion of their flight powered), with relatively large flight muscles (also usual). The mallard's wings are thin and pointed, giving it high aspect ratio (and hence difficulty in obtaining lift in slow flight) while the pheasant has broad rounded wings of low A_r implying good take-off capacity and poor performance in fast flight. These characteristics are well illustrated by the power curves; the power per unit mass is much lower for the mallard than for the pheasant, and also power increases more slowly at high speeds for the mallard; its preference for fast flight compared to the pheasant's preference for slow flight is clear from its lower aerodynamic power at high speeds.

These arguments indicate the critical effect of avian morphology on flight proficiency; similar deductions may be made for other species, and we may be confident that the model will confirm their validity. It remains for us to discuss how the bird can better its flight proficiency at different speeds by a judicious choice of morphological parameters. The animal can gain access to the envelope of the accessible power curves in the same way that a gliding bird can reach the envelope of its glide polars by, for instance, spreading its wings at low velocities. There is some benefit from reducing profile power at high speeds by reducing ϕ and increasing τ as far as is possible, but hitherto we have assumed that the stroke period and the morphological parameters are constant at all speeds. Any changes in body mass M as a result of fat consumption would be slow, although for very small birds on long flights can be significant; it is unlikely that wing chord c_0 could be changed, but on the other hand wing semi-span b can (and probably does) vary, and some species at least can vary T. Assuming that all other parameters are unchanged, we find that, very broadly, induced power is proportional to Tb^{-3}, and profile power to b^4T^{-3}. There is therefore a clear preference for large span and small period for slow flight, and for small span and large period in fast flight. If a bird can adapt in this way (as far as is consistent with the needs of lift generation and with anatomical constraints) its choice of flight mode will be broad, although it is the way of things that it is likely to have a high power to weight ratio in return for its flexibility. An example of a bird which has this broad flexibility is the pigeon; the remaining four species we selected have each evolved a strong preference

for a single flight style; the wren for short darting flight, the flycatcher for agility and hovering, the duck for fast flight and the pheasant for a rapid escape from its predators.

5. DIMENSIONAL SCALING AND FORWARD AVIAN FLIGHT

A powerful tool in discussions of animal flight is dimensional scaling, used to express broadly the variation of body dimensions with size over a wide range of species. This can indicate the relative magnitudes or effects of different factors in a problem, can estimate unknown quantities when few exact values are known, or, most instructively, can suggest how variations on or departures from the rules of scaling in a single species or group of species may be of some evolutionary advantage. We have used these arguments to ignore inertial power in avian forward flight as negligible compared with the other components, and to estimate parasite drag from a small number of measurements. We now discuss the implications of the vortex ring model for birds of differing sizes.

The basic principles of isometric scaling, in which all birds are assumed to have the same body proportions, so that for instance wing span is proportional to mass to the power one-third, and wing area to mass to the power two-thirds, have been set out by Greenewalt (1962) and Pennycuick (1968, 1969). More detailed applications of the arguments to various topics in animal locomotion will be found in the proceedings of a recent conference on the topic (Pedley, 1977).

According to isometric scaling all lengths scale similarly, so that for instance $b \propto M^{\frac{1}{3}}$, $S \propto M^{\frac{2}{3}}$, $m_p \propto M$; aspect ratio is constant and disc loading $N_d \propto M^{\frac{1}{3}}$. From simple arguments we can readily deduce that the characteristic flight speeds V_0, V_1 scale as mass to the one-sixth power, and power consumption at these speeds as mass to the seven-sixths power, that is

$$\left.\begin{aligned} V_0, V_1 &\propto M^{\frac{1}{6}}, \\ P_0 &\propto M^{\frac{7}{6}}. \end{aligned}\right\} \tag{25}$$

Cost of transport is physically a dimensionless quantity, and therefore, on this simple theory, should be constant. Any dimensionless quantity should remain constant over the whole range of body masses if isometric scaling applies, but as we shall see later, this is not normally the case. We also expect stroke period to scale as the one-sixth power of mass if profile and parasite powers are to behave similarly; this is probably inconsistent with muscle dynamics (Goldspink, 1977) and does not usually apply (Weis-Fogh, 1977). Muscle dynamics impose a limit to the maximum power output (P_a) proportional to body mass (Weis-Fogh & Alexander, 1977), which in connexion with (25) above implies a maximum size above which flight is not possible; calculations suggest that this size corresponds to that of the largest flying animals, about 10 kg (swans, bustards, albatrosses, condors).

Greenewalt (1962) assembles a vast mass of data on flying animals of all kinds, and shows that it conforms well to isometric scaling. This is to be expected, since there is remarkably little variation in body proportions in the classes Insecta or Aves compared with, say, in the Mammalia. In particular he quotes a body of data from Magnan (1922) that is still the broadest and most useful set of bird measurements; an additional source of data is Fullerton (1911), although these figures were collected from a number

Table 4. *Dimensional scaling of flying birds, after Greenewalt* (1962, 1975)

(All quantities in MKS units (stroke period T in s). For details of the birds contained in the groups passeriform, shorebird, duck, see Greenewalt (1975). Feathering parameter is shown divided by T^2.)

	Interspecific or isometric scales	Intraspecific or allometric scales		
		Passeriform	Shorebird	Duck
Semi-span, b	$0{\cdot}55M^{\frac{1}{3}}$	$0{\cdot}66M^{0{\cdot}42}$	$0{\cdot}58M^{0{\cdot}40}$	$0{\cdot}47M^{0{\cdot}41}$
Wing area, S	$0{\cdot}157M^{\frac{2}{3}}$	$0{\cdot}22M^{0{\cdot}79}$	$0{\cdot}13M^{0{\cdot}71}$	$0{\cdot}08M^{0{\cdot}71}$
Aspect ratio, A_r	$7{\cdot}7$	$7{\cdot}98M^{0{\cdot}05}$	$10{\cdot}4M^{0{\cdot}09}$	$10{\cdot}5M^{0{\cdot}10}$
Disc loading, N_d	$10{\cdot}3M^{\frac{1}{3}}$	$7{\cdot}15M^{0{\cdot}14}$	$9{\cdot}28M^{0{\cdot}19}$	$14{\cdot}4M^{0{\cdot}18}$
Pectoral muscle mass, m_p	$0{\cdot}155M$	$0{\cdot}161M^{0{\cdot}97}$	$0{\cdot}20M^{0{\cdot}97}$	$0{\cdot}20M^{0{\cdot}97}$
Muscle ratio, μ	$1{\cdot}10$	$1{\cdot}087$	$1{\cdot}087$	$1{\cdot}087$
Momentum jet induced power, $P_{i,M}$	$20{\cdot}2M^{\frac{7}{9}}$	$16{\cdot}8M^{1{\cdot}08}$	$19{\cdot}1M^{1{\cdot}10}$	$23{\cdot}8M^{1{\cdot}10}$
Feathering parameter, f/T^2	$1{\cdot}42M^{-\frac{1}{3}}$	$0{\cdot}68M^{-0{\cdot}68}$	$1{\cdot}15M^{-0{\cdot}61}$	$2{\cdot}76M^{-0{\cdot}64}$

of sources and probably reflect different measuring techniques. On the basis of Magnan's data, Greenewalt has derived the form of the isometric scaling relations for the birds; these have been re-expressed in terms of body mass, in MKS units throughout, and are shown in the first column of Table 4. Greenewalt's stroke period data seem unreliable and are omitted. The standard errors of these figures are not known, but in view of the isometric assumption they are probably relatively large.

In a more recent paper, Greenewalt (1975) has considered the same data in the light of allometric scaling. This assigns a relation of the form

$$\ln b = \alpha + \alpha' \ln M \tag{26}$$

between wing semi-span and body mass (and similarly for other pairs of parameters). The constants α, α' depend on the units of b and M, and are determined by linear regression on real data. If isometric scaling applied α' would be $\frac{1}{3}$ in this case. Greenewalt has rationalized the possible consequences of departures from isometricity in individual species by dividing the birds into three groups (models), based largely on disc loading: passeriformes, shorebirds and ducks. The division is related more to the animal's geometry than to taxonomy, but is helpful. His regression results, recalculated to MKS units and put into a consistent form, are given in Table 4. The most important implication is the faster increase of wing span with size than is expected, with therefore a lower disc loading and feathering parameter. The intention is reduction of induced power for larger birds ($P_i \propto M^{1{\cdot}1}$ compared with $M^{\frac{7}{9}}$), facilitating take-off and lift generation in slow flight. With their high wing loading it is not surprising that birds in the duck model experience difficulty in taking off (e.g. mallard).

This approach of Greenewalt's suggests that much can be learnt from considering scaling purely within a taxonomically similar group of birds; the range of masses would be small so that a large number of measurements would be required for good statistical accuracy. Because of the differing evolutionary answers to scaling problems we need not expect the same trend with a small group of species (or even a single species) as with the birds as a whole. For instance, Greenewalt (1962) found that wing semi-span scales closely to $\frac{2}{3}$ within the hummingbirds compared with the expected $\frac{1}{3}$

Table 5. *Allometric scaling of stroke period and of feathering parameter f (based on formulae in Table 4)*

(All quantities in MKS units.)

	Interspecific rule (all birds)	Intraspecific rules		
		Passeriforms	Shorebirds	Ducks
Size of sample	167	115	33	19
Stroke period, T	$0{\cdot}27M^{0{\cdot}29}$	$0{\cdot}33M^{0{\cdot}28}$	$0{\cdot}25M^{0{\cdot}19}$	$0{\cdot}17M^{0{\cdot}24}$
Feathering parameter, f	$0{\cdot}103M^{0{\cdot}25}$	$0{\cdot}074M^{0{\cdot}05}$	$0{\cdot}070M^{-0{\cdot}24}$	$0{\cdot}083M^{-0{\cdot}16}$

found overall, and Weis-Fogh (1977) found differing scaling rules for the stroke period in insects. Warham (1977) has shown in the Procellariiformes (petrels and albatrosses), over a size range from 20 g up to nearly 10 kg, that $S \propto M^{0{\cdot}59}$, a considerably lower rate of increase than we would expect, which probably reflects the good soaring capabilities of albatrosses which have long wings of very high aspect ratio. A similar approach has been made by Oehme *et al.* (1977) using linear as opposed to log-linear regression, so no comparison may be made.

Data for the morphological parameters are widely available in the literature; they must be used with some caution because of the difficulty of reconciling observations by different authors, and because the physical condition of the bird (e.g. tired, ill, well fed, before or after long flights) is rarely, if ever, mentioned. There is, however, very little information on the variation of stroke period T with body size. With modern stroboscopic or radar techniques the determination of T is straightforward; ideally it can be made in common with measurements of morphological data. Older measurements were rarely made with any great degree of sophistication and cannot be relied upon. What data there are to be found in the literature have been collected and subject to log-linear regression. Where no body mass is quoted this has been found from Greenewalt (1962). Among the sources used are Berger, Roy & Hart (1970), Bruderer, Jacquat & Brückner (1972), Cone (1968), Greenewalt (1962), Herzog (1968) and Oehme & Kitzler (1974). The resulting scaled relations are given in Table 5 and Fig. 10.

The standard errors of the formulae in Table 5 are large, and we cannot expect the estimates to be very accurate. The overall trend towards a $M^{\frac{1}{4}}$ rule rather than to the aerodynamically consistent $M^{\frac{1}{6}}$ is evident. In the absence of better measurements, the formulae quoted do allow estimation of T if M is known. The rapid rise in T combines with the rapid rise in semi-span b in the passeriform model to make f nearly constant, so that induced power is low and hence take-off and slow flight for the larger birds are facilitated. In the shorebirds and ducks the rise in T is slower, and f actually decreases with size; even with their much smaller wings these birds are capable of getting into the air.

This method of determination of the $T(M)$ relation tacitly assumes that T is fixed for any particular species; it would be determined by the various anatomical sizes and dimensions in such a way that it can be considered as one of the morphological parameters. Stroke period *is* constant among the insects because the thorax stores elastic energy; the period is the resonant period of the system. Greenewalt (1960, 1975) argues that the constant periods observed in hummingbirds and birds imply the

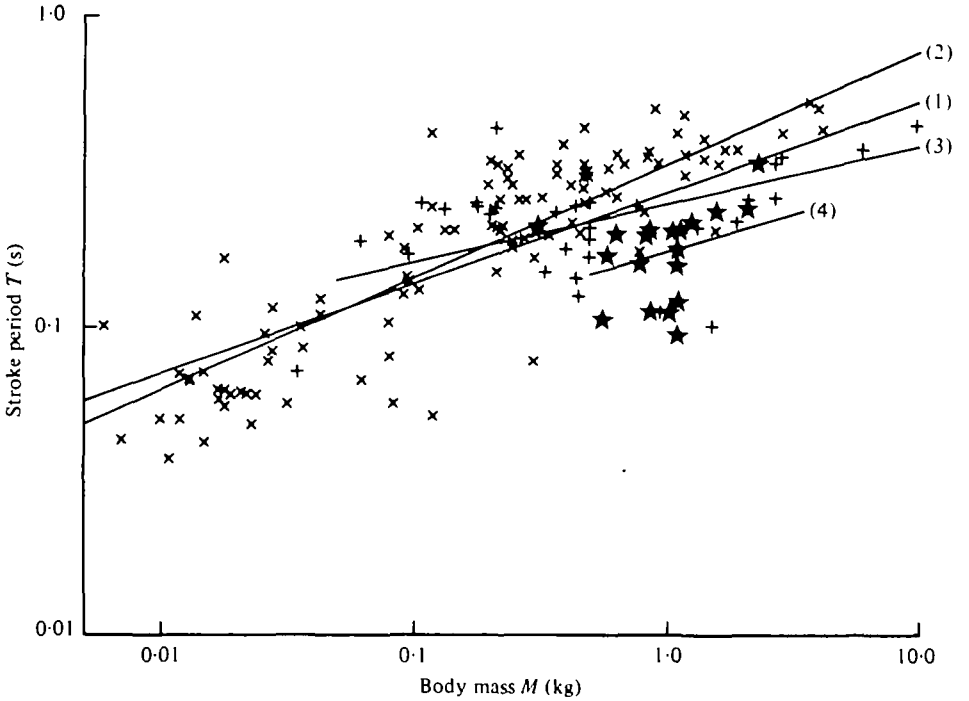

Fig. 10. Observed stroke period plotted against body mass (various sources) with calculated regression lines. ×, Passeriforms; +, shorebirds; ★, ducks. (1) All data, $T = 0{\cdot}27M^{0{\cdot}29}$; (2) passeriforms: $T = 0{\cdot}33M^{0{\cdot}26}$; (3) shorebirds, $T = 0{\cdot}25M^{0{\cdot}19}$; (4) ducks, $T = 0{\cdot}17M^{0{\cdot}24}$. See section 5 for interpretation of these data.

presence of an elastic system, but Weis-Fogh (1972) failed to find it. Schaefer (1975) suggests that the clavicle in most birds can store energy; in fact this would not be possible; the natural frequency is too high and the bone is not strong enough to store the energy involved, and moreover many upright standing birds (owls, parrots) have two separate furculae which are not fused to form a single clavicle.

It is by no means clear that the stroke period is fixed in most birds, and indeed there is some evidence that it is not; Greenewalt does not justify his claim that constant values may be taken. As mentioned in section 4, Oehme (1968) and Tucker (1972) have observed changes in flight style between slow and fast forward flight. As we have seen these are of distinct advantage in energy reduction, and there is no reason to assume that similar changes do not take place in other species. Pennycuick (1968) records a tendency for T to increase as speed increases in the pigeon.

No doubt there are some birds for which the assumption of constant period is justified (probably many small passerines); there is definite evidence that it remains remarkably constant in hummingbirds. Since vertebrate flyers have no suitable elastic resonance we must suggest an alternative reason. Of course, there may be no *need* to vary T, although the power calculations in section 4 suggest that this is unlikely. One possibility is some form of aerodynamic effect related to unsteady lift generation; this topic is ill-understood, so the idea can be no more than speculation. A more likely suggestion is a preferred muscular contraction rate (or velocity) at which the chemical efficiency of the muscles and the mechanical efficiency of the tendons and joints is

maximum. If such an optimum efficiency were pronounced it could be a further reason for intermittent or bounding flight (Rayner, 1977). One might further hypothesize that the variations in muscle fibre between species are related to the degree of flexibility in stroke period the animal enjoys: as a mathematician this author is not competent to explore this topic!

It is evident that much attention needs to be given to stroke period by ornithologists skilled in observational work. It would be of inestimable value if a programme of observations of both kinematic and morphological parameters for a large number of species in a variety of flight conditions was carried out. Much of the present work has been hampered by lack of adequate data. In the power calculations described in this paper a constant value for the period has been used in all flight conditions, derived either from observation or from Table 5. In slow flight or hovering we might expect a lower value, with a higher value in fast forward flight.

We now consider the variation of flight velocity and flight power with body mass; we consider minimum power and maximum range (minimum cost) speeds V_0 and V_1, minimum flight power $P_0 = P(V_0)$ and minimum cost of transport C_1. Pennycuick (1969) gives speed ranges for a variety of animals by using Greenewalt's data; since all the terms in his expression scale equally it is not surprising that flight speeds correspond to the isometric $M^{\frac{1}{6}}$ power rule. In the vortex ring model this is not the case, and we will find important departures from isometric scaling. Greenewalt (1975) attempted to discuss such departures, but used a crude power model which cannot be justified aerodynamically, so that his results cannot be considered reliable.

The results for the four quantities are shown in Table 6 and Figs. 11–14. All calculations were performed with $\phi = 120°$ and $\tau = \frac{3}{7}$, and with drag given by (19) and (20) as in the calculations described in section 4; this is a realistic configuration for fast forward flight ($V \geqslant V_0$). The calculations are in two groups. First, with scaled approximations for the morphological parameters calculated from Greenewalt (1975), and set out in Table 4, with stroke period given in Table 5; these are referred to as 'ideal' power and velocity scalings. Secondly, with real data for 68 birds (44 passeriform, 15 shorebird, 9 duck) mainly from Greenewalt (1962). The latter 'real' calculations are illustrated in Figs. 11–14; in these figures the lines drawn represent regression on all 68 points, as in the second row of Table 6. In all figures diagonal crosses represent passeriforms, horizontal crosses shorebirds, and stars ducks.

It is clear from Table 6 that there is no significant difference between real and ideal results in most cases; discrepancies in the figures for ducks may be explained by the small amount of available data, since the results are not statistically significant.

The first row of Table 6 shows the results of ideal isometric scaling; power P_0 and cost C_1 are close to the theoretical behaviours of proportionality to $M^{\frac{1}{6}}$ and constant respectively, but the velocities increase rather faster than $M^{\frac{1}{6}}$. The penalty for high velocity, and the reason why birds are not isometrically scaled, is the high power required, which is too great for larger animals. Real data for all kinds of birds show a slower increase in speed with mass, so that larger birds fly slower than in the ideal case, with compensating power reduction. The cost of transport in these (and all other) cases is around 0·2, decreasing gradually as mass increases, reflecting the better gliding capacities of large birds.

Within each of the three groups of Greenewalt's model (passeriform, shorebird,

Table 6. *Relation of power and flight speed to body mass for vortex ring model, calculated using ideal scaling from Greenewalt (Table 4) and also from real data*

(No statistically significant variation between the cases except in the interspecific rule, where ideal scaling refers to isometricity.)

	Minimum power speed, V_0	Minimum cost speed, V_1	Minimum power, $P_0 = P_0(V_0)$	Minimum cost, $C_1 = P(V_1)/Mg\,V_1$
Interspecific rules				
Greenewalt (1962)	$5{\cdot}72M^{0{\cdot}30}$	$10{\cdot}04M^{0{\cdot}34}$	$16{\cdot}14M^{1{\cdot}16}$	$0{\cdot}225M^{-0{\cdot}05}$
Real data all birds	$5{\cdot}70M^{0{\cdot}16}$	$10{\cdot}89M^{0{\cdot}19}$	$15{\cdot}38M^{1{\cdot}10}$	$0{\cdot}212M^{-0{\cdot}07}$
Intraspecific rules				
Passeriformes				
Greenewalt	$4{\cdot}17M^{0{\cdot}11}$	$7{\cdot}75M^{0{\cdot}11}$	$12{\cdot}59M^{1{\cdot}05}$	$0{\cdot}215M^{-0{\cdot}07}$
Real data	$5{\cdot}04M^{0{\cdot}18}$	$8{\cdot}63M^{0{\cdot}14}$	$12{\cdot}93M^{1{\cdot}05}$	$0{\cdot}205M^{-0{\cdot}08}$
Shorebirds				
Greenewalt	$5{\cdot}32M^{0{\cdot}09}$	$8{\cdot}98M^{0{\cdot}03}$	$14{\cdot}51M^{1{\cdot}07}$	$0{\cdot}222M^{-0{\cdot}001}$
Real data	$5{\cdot}85M^{0{\cdot}10}$	$10{\cdot}49M^{0{\cdot}06}$	$15{\cdot}35M^{1{\cdot}07}$	$0{\cdot}209M^{-0{\cdot}02}$
Ducks				
Greenewalt	$6{\cdot}13M^{0{\cdot}10}$	$12{\cdot}43M^{0{\cdot}01}$	$19{\cdot}36M^{1{\cdot}06}$	$0{\cdot}248M^{-0{\cdot}007}$
Real data	$6{\cdot}78M^{0{\cdot}22}$	$17{\cdot}12M^{0{\cdot}01}$	$20{\cdot}84M^{1{\cdot}14}$	$0{\cdot}229M^{-0{\cdot}08}$

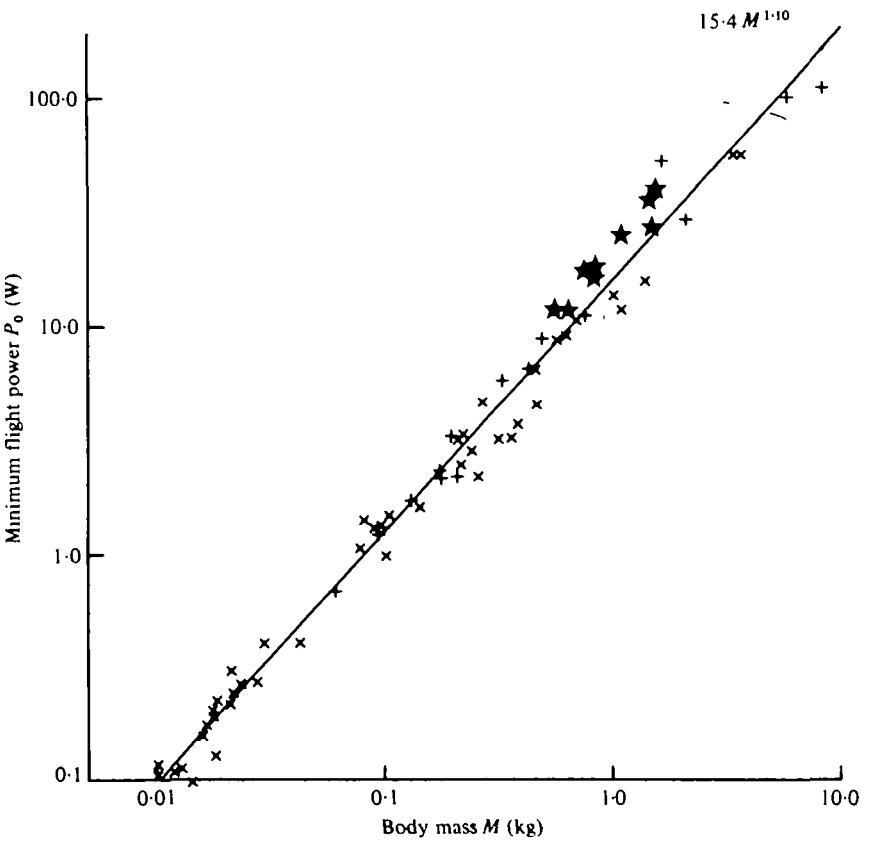

Fig. 11. Minimum flight power P_0 plotted against body mass, with regression line for all this data. Note tendency for larger passeriforms (×) to fall below line, with ducks (★) consistently just above. Little distinction can be traced between shorebirds (+) and passeriforms in the larger size range.

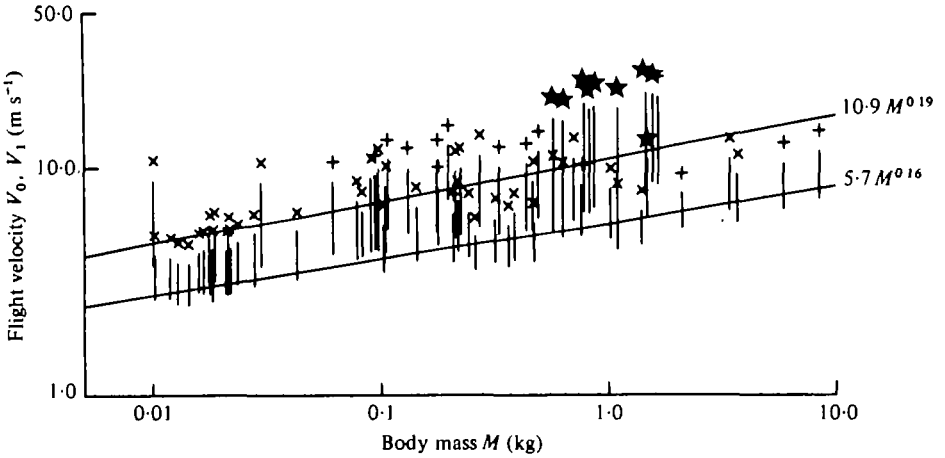

Fig. 12. Optimum flight velocities V_0 and V_1 plotted against body mass, with regression line for all this data. Vertical lines join V_0 and V_1 for each bird; symbol above each line signifies type of bird. Note high flight speeds of all ducks, and tendency for other large birds to have relatively low flight speeds.

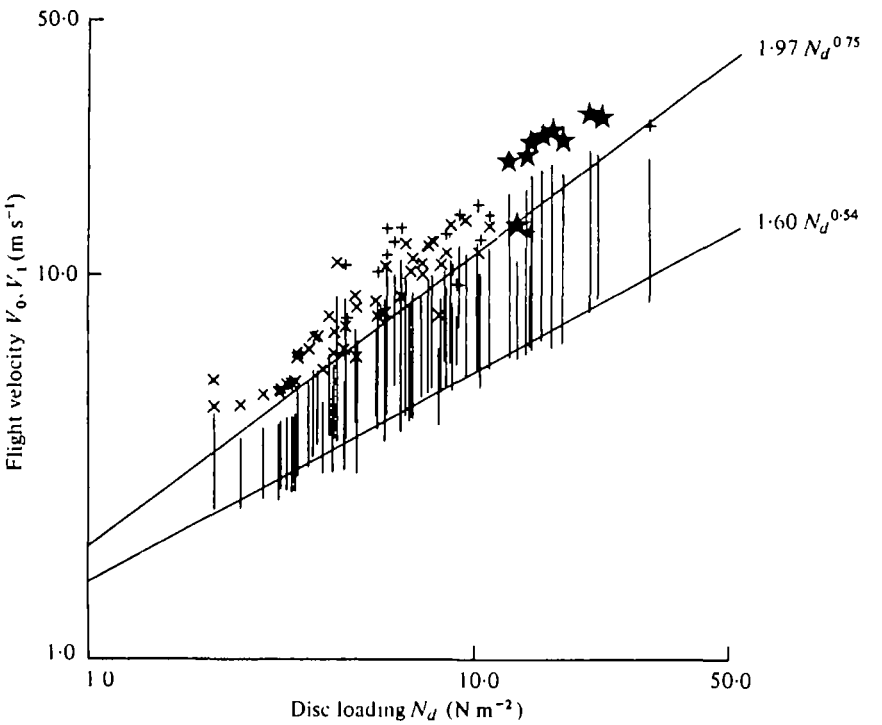

Fig. 13. Optimum flight velocities V_0 and V_1 plotted against disc loading N_d. Shows that flight speed correlates closely with disc loading (compare Fig. 12, where the scatter is far greater). Note increase in speed range ($V_1 - V_0$) with disc loading, since V_1 is less dependent on induced power (and hence on N_d) than is V_0.

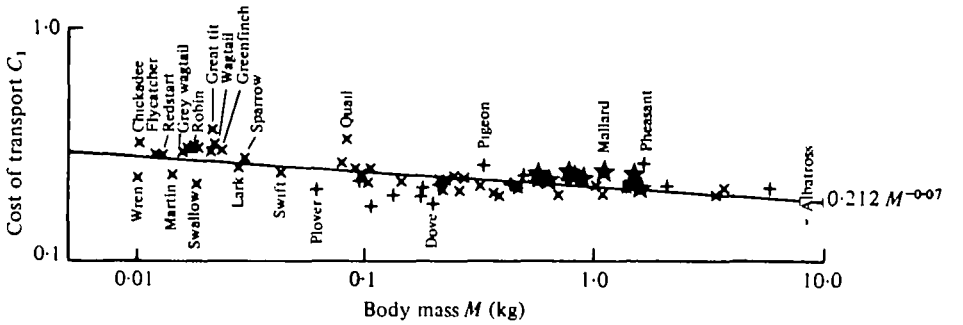

Fig. 14. Minimum cost of transport C_1 plotted against body mass. Shows that the effect of anomalies is to cause C_1 to fall as mass rises. Note consistently low values for martin, swift, etc., which do not use bounding flight, compared to higher values for passerines falling above line which do. Brief English names of some birds only are given.

duck) we see that the effect of dimensional anomalies is to reduce flight power and flight speed for larger birds compared with the isometric results, while keeping cost of transport down. This is evidently the optimum course, for power consumption is more critical for large birds than for small (the wren is an exception in this respect), and large birds do not need to fly fast provided cost of transport is low enough to give them a good migratory range. These conclusions are of course generalizations, but confirm that the course evolution has taken is *aerodynamically* beneficial. As we would expect from their higher wing loadings, shorebirds and ducks have both higher flight speeds and powers, and yet retain low costs of transport. The range of masses for which this policy of increasing wing loading to obtain higher speeds is useful will be bounded above and below by limits of muscular contraction and lift generation in take-off, and accounts for the absence of any shorebird weighing less than 0·035 kg or any duck less than 0·2 kg or greater than 2 kg. The majority of ducks fall into a narrow range about 1 kg.

Greenewalt (1975) suggested that disc loading N_d was a significant parameter. We see immediately from (4) and (9) that in slow flight this must be so, because induced power and (hovering) induced velocity are closely related to it. Comparing Figs. 12 and 13, where velocities are shown against mass and against disc loading N_d, we immediately see that the correlation of flight velocity to disc loading is much better than to mass; V_0 correlates better than V_1, since induced effects are more important at lower speeds. Power and cost of transport (shown against mass in Figs. 11 and 14) do not fit closely with disc loading; there is too much scatter to allow any inference to be made.

The tendency for minimum cost speed V_1 to increase very slowly with mass in the shorebirds and ducks is interesting. It is a consequence of the high disc loadings of these species that there is a very shallow minimum in the $P(V)$ curve. Although V_1 is low in the larger species, these birds can often achieve much greater speeds with only modest increase in power. The mallard is reported to be among the fastest of all flying vertebrates. Large passeriforms (e.g. birds of prey) tend to have large wings, and obtain high velocities by gliding or using undulating flight (a mixture of flapping and gliding).

Many small passerines have low disc loadings, and their profile power is large at around speed V_1. The power required in fast flight increases rapidly with speed, so that cost of transport is high. For many of these species the power output for sustained forward flight at speed V_1 will be more than their muscles can provide. The solution to this difficulty is bounding flight, when the wings beat for a portion of the flight time and are otherwise folded against the body. To birds with low disc loading and high profile drag this strategy with its characteristic sinusoidal path produces a substantial energy saving (Rayner, 1977). We would expect to find it in passeriform birds with a high cost of transport, that is in those falling above the regression line in Fig. 14. It can be expected, and is indeed observed, in such families as the tits (Paridae), finches (Fringillidae), warblers (Muscicapidae) and sparrows (Ploceidae), but not in the wren with its tiny wings, or in swallows, swifts and martins (Hirundinidae), with long wings but large stroke period and therefore low profile power. The quail, with small wings and a very low stroke period, is exceptional and would gain no benefit from bounding flight. The largest birds using this strategy are the woodpeckers (mass 0·3 kg), but unfortunately no data for these species were available.

Another form of energy saving used by large birds of high disc loading (e.g. geese) is formation flight. Although we do not consider this, the extension of the vortex ring model to this topic would be relatively simple.

As in all problems concerned with natural flight, power optimization involves a large number of independent factors which often operate countrary to one another. Dimensional scaling tends to smooth out this problem, but its conclusions can only be as good as the input data, and it is to this topic that much attention must be given.

6. CONCLUSIONS

1. Existing theories of animal flight are based on a number of assumptions which are not tenable aerodynamically. A theory which does not use lift or drag coefficients, and which does not derive induced power from the unsatisfactory actuator disc and momentum jet theory, is put forward. This theory gives a good description of the mechanism by which hovering of birds and insects and forward flight of birds takes place, and permits calculation of flight power.

2. The wake in the hovering flight of insects and hummingbirds (normal hovering) and of birds (avian hovering, when only the downstroke generates aerodynamic forces) is a chain of vertically stacked circular vortex rings each shed by a single wing-stroke. The momentum associated with each ring must be sufficient to support the animal for the time interval between generation of rings. A tilted stroke plane is necessary if wake momentum is to be vertical.

3. The configuration of the vorticity distribution in the wake depends on two non-dimensional parameters. The feathering parameter f depending on the animal's morphology and the initial ring radius depending on assumed wing circulation. For small values of f the wake is similar to the momentum jet wake; as f increases (as mass increases) the spacing between adjacent vortex rings increases, and the assumptions of mass and momentum conservation within the wake are no longer satisfactory.

4. The induced power in hovering is the rate of doing work adding additional vortex rings to the chain. A simple expression is given to assist with its calculation.

The momentum jet generated by an actuator disc of radius equal to the initial radius of each vortex ring gives a good estimate of the induced power in normal hovering; we deduce that in normal hovering tip losses are small. In avian hovering tip losses are much greater.

5. The strategy an animal should choose to hover most efficiently is to reduce stroke period and increase stroke amplitude as far as is consistent with the body structure, unless an unfavourable increase in profile power results.

6. The wake in the forward flight of birds is modelled by a chain of elliptical vortex rings. This configuration is consistent with wing motions and the aerodynamics of reciprocating wings. Photographic evidence (Magnan) suggests that vortex rings are present.

7. The momentum of each vortex ring in steady level forward flight must overcome parasite and profile drags in addition to body weight. Power consumption in forward flight is the sum of induced power, calculated as the increment of wake momentum, parasite, and profile power.

8. Induced power is dominant in slow flight, but falls away rapidly. Parasite and profile powers are small in slow (avian) flight and gradually increase. The curve of power against velocity is U-shaped.

9. The power curve allows definition of two characteristic speeds, at which the work done per unit time and per unit distance are minimized. This represents the aerodynamic power required. The true cost to fuel reserves depends on efficiency of energy conversion in the muscles, which is probably velocity-dependent. No comparisons should be made with physiological power measurements without considering the effect of varying efficiency.

10. The pattern of kinematic parameters that a bird in forward flight may choose is described as flight style, which varies with flight mode. The range of kinematic parameters available is limited by the properties of the muscles concerned, in addition to the velocity-dependent constraint of lift and thrust generation. The bird must select the parameters within these limits that minimize the rate of working; in slow flight a large, rapid downstroke is needed, in fast flight as small a downstroke as possible. Total power consumption must be within the range at which the muscles can work aerobically if flight is continuous.

11. Some broad rules describing the relation between morphology and flight style are evident, and are confirmed in detail by the model. A bird with low stroke period and/or large wing span (that is, low feathering parameter) is better equipped to fly slowly or to hover than one for which feathering parameter and aspect ratio are high which should prefer fast flight. Many small passerines violate this latter condition, and in general so have relatively high parasite drag; they can obtain high flight speeds at smaller energy cost by adopting bounding flight; this is most prevalent among passerines with low disc loading and low feathering parameter, and which therefore would have high cost of transport.

12. By choosing kinematic parameters within certain constraints a bird gains access to the envelope of a family of power curves; the optimum strategy is to use a slow, small amplitude in fast flight and long amplitude in short flight. If in addition the wing span and stroke period can be varied – which is probably the case in some,

but not all, species – it should reduce span and increase period at high velocities. Observations confirm that this behaviour does indeed take place.

13. If it is meaningful to consider stroke period as fixed for any bird, then this period may be related to body mass if a large enough body of data is available. Linear regression on data for 167 birds suggests that stroke period increases as $(\text{mass})^{0.29}$, that is considerably faster than suggested by isometric aerodynamic scaling arguments.

14. Power consumption related to body mass by allometric scaling does not show any significant difference between results for real data for 68 birds and ideal scaled morphological data. Body dimensions differ from isometric scales in such a way that larger birds have a lower cost of transport, so that take-off and slow flight are practical without exorbitant induced power demands. Large birds do not need to fly fast, although high disc loading permits high flight speeds with a greater power cost. All anomalies in dimensional scaling reflect the exorbitant cost of lift generation in slow flight for large birds.

15. Several points of uncertainty in the theory would benefit from experimental attention. Flow visualization studied for both insects and birds will clarify the geometry of the vortex wake, and should give insight into the mechanism of vortex ring formation. Observations of kinematic parameters, and particularly of stroke period, and measurements of parasite drag are of particular importance. Without additional data of this kind there is little scope for further theoretical work, although attention might be given to unsteady lift generation when the clap-and-fling cannot be of assistance.

The author wishes to express his appreciation for the great deal of help and assistance he has received in the course of this work, and especially from Professor Sir James Lighthill, F.R.S., C. P. Ellington and Dr K. E. Machin. He acknowledges the financial support of the Science Research Council.

REFERENCES

BATCHELOR, G. K. (1967). *An Introduction to Fluid Dynamics*. Cambridge University Press.

BERGER, M., ROY, O. Z. & HART, J. S. (1970). The coordination between respiration and wing beats in birds. *Z. vergl. Physiol.* **66**, 190–200.

BROWN, R. H. J. (1963). The flight of birds. *Biol. Rev.* **38**, 460–489.

BRUDERER, B., JACQUAT, B. & BRÜCKNER, U. (1972). Zur bestimmung von Flügelschlagfrequenzen tag- und nachtziehender Vogelarten mit Radar. *Orn. Beob.* **69**, 189–206.

CONE, C. D. Jr. (1968). The aerodynamics of flapping birdflight. *Spec. scient. Rep., Va Inst. mar. Sci.* **52**.

COOTER, R. J. & BAKER, P. S. (1977). Weis-Fogh clap and fling mechanism in *Locusta*. *Nature, Lond.* **269**, 53–54.

CSICSÁKY, M. J. (1977). Body-gliding in the zebra finch. *Fortschr. Zool.* **24**, 275–286.

ELLINGTON, C. P. (1978). The aerodynamics of normal hovering flight. In *Comparative Physiology – Water, Ions and Fluid Mechanics* (ed. K. Schmidt-Nielsen, L. Bolis and S. H. P. Maddrell), pp. 327–345. Cambridge University Press.

FULLERTON, J. D. (1911). *Aeronautical Society of Great Britain: First report of bird construction committee*. London: Aeronautical Society.

GOLDSPINK, G. (1977). Mechanics and energetics of muscle in animals of different sizes, with particular reference to the muscle fibre composition of vertebrate muscle. In Pedley (1977), pp. 37–55.

GREENEWALT, C. H. (1960). The wings of birds and insects as mechanical oscillators. *Proc. Am. phil. Soc.* **104**, 605–611.

GREENEWALT, C. H. (1962). Dimensional relationships for flying animals. *Smithson. misc. Collns* **144**, 2.

GREENEWALT, C. H. (1975). The flight of birds. *Trans. Am. phil. Soc.* **65**, 4.

HERZOG, K. (1968). *Anatomie und Flugbiologie der Vögel.* Stuttgart: Gustav Fischer Verlag.
HOFF, W. (1919). Der Flug der Insekten. *Naturwissenschaften* **7**, 159–164.
HUMMEL, D. & MÖLLENSTÄDT, W. (1977). On the calculation of the aerodynamic forces acting on a house sparrow (*Passer domesticus*) during downstroke by means of aerodynamic theory. *Fortschr. Zool.* **24**, 235–256.
LIGHTHILL, M. J. (1973). On the Weis-Fogh mechanism of lift generation. *J. Fluid Mech.* **60**, 1–17.
LIGHTHILL, M. J. (1977). Introduction to the scaling of aerial locomotion. In Pedley (1977), pp. 365–404.
MAGNAN, A. (1922). Les caractéristiques des oiseaux suivant le mode de vol. *Annls Sci. nat.* Sér. 10, **5**, 125–234.
MAGNAN, A., PERRILLIAT-BOTONET, C. & GIRARD, H. (1938). Essais d'enregistrements cinématographiques simultanées dans trois directions perpendiculaires deux à deux de l'écoulement de l'air autour d'un oiseau en vol. *C. r. hebd. Séanc. Acad. Sci. Paris.* **206**, 462–464.
NORBERG, U. M. (1975). Hovering flight in the pied flycatcher (*Ficedula hypoleuca*). In *Swimming and Flying in Nature*, vol. 2 (ed. T. Y. Wu, C. J. Brokaw and C. Brennen), pp. 869–881. New York: Plenum Press.
NORBERG, U. M. (1976*a*). Aerodynamics, kinematics and energetics of horizontal flight in the long-eared bat *Plecotus auritus*. *J. exp. Biol.* **65**, 179–212.
NORBERG, U. M. (1976*b*). Aerodynamics of hovering flight in the long-eared bat *Plecotus auritus*. *J. exp. Biol.* **65**, 459–470.
OEHME, H. (1968). Der Flug des Mauerseglers (*Apus apus*). *Biol. Zbl.* **88**, 287–311.
OEHME, H., DATHE, H. H. & KITZLER, U. (1977). Research on biophysics and physiology of bird flight. IV. Flight energetics in birds. *Fortschr. Zool.* **24**, 257–273.
OEHME, H. & KITZLER, U. (1974). Untersuchungen zur Flugbiophysik und Flugphysiologie der Vögel. I. Über die Kinematik des Flügelschlages beim unbeschleunigten Horizontalflug. *Zool. Jb. Physiol.* **78**, 461–512.
OEHME, H. & KITZLER, U. (1975*a*). Untersuchungen zur Flugbiophysik und Flugphysiologie der Vögel. II. Zur Geometrie des Vögelflügels. *Zool. Jb. Physiol.* **79**, 402–424.
OEHME, H. & KITZLER, U. (1975*b*). Untersuchungen zur Flugbiophysik und Flugphysiologie der Vögel. III. Die Bestimmung der Muskelleistung beim Kraftflug der Vögel aus kinematischen und morphologischen Daten. *Zool. Jb. Physiol.* **79**, 425–458.
OSBORNE, M. F. M. (1951). Aerodynamics of flapping flight with applications to insects. *J. exp. Biol.* **28**, 221–245.
PEDLEY, T. J. (ed.) (1977). *Scale Effects in Animal Locomotion.* London: Academic Press.
PENNYCUICK, C. J. (1968). Power requirements for horizontal flight in the pigeon *Columba livia*. *J. exp. Biol.* **49**, 527–555.
PENNYCUICK, C. J. (1969). The mechanics of bird migration. *Ibis* **111**, 525–556.
PENNYCUICK, C. J. (1975). Mechanics of flight. In *Avian biology*, vol. 5 (ed. D. S. Farnell, J. R. King and K. C. Parkes). London: Academic Press.
RAYNER, J. M. V. (1977). The intermittent flight of birds. In Pedley (1977), pp. 437–443.
RAYNER, J. M. V. (1979*a*). A vortex theory of animal flight. I. The vortex wake of a hovering animal. *J. Fluid Mech.* (in the Press).
RAYNER, J. M. V. (1979*b*). A vortex theory of animal flight. II. The forward flight of birds. *J. Fluid Mech.* (in the Press).
SCHAEFER, G. W. (1975). Dimensional analysis of avian forward flight. Symposium on Biodynamics of Animal Locomotion, Cambridge, September 1975. (Unpublished.)
SPILLMAN, J. (1979). The use of wing tip sails to reduce vortex drag. *J. R. aero. Soc.* (in the Press).
TUCKER, V. A. (1972). Metabolism during flight in the laughing gull *Larus atricilla*. *Am. J. Physiol.* **222**, 237–245.
TUCKER, V. A. (1973). Bird metabolism during flight: evaluation of a theory. *J. exp. Biol.* **58**, 689–709.
TUCKER, V. A. (1977). Scaling and avian flight. In Pedley (1977), pp. 497–509.
VOGEL, S. (1967). Flight in *Drosophila*. III. Aerodynamic characteristics of fly wings and wing models. *J. exp. Biol.* **46**, 431–443.
WARHAM, J. (1977). Wing loadings, wing shapes and flight capabilities of Procellariiformes. *N.Z. Jl Zool.* **4**, 73–83.
WEIS-FOGH, T. (1972). Energetics of hovering flight in hummingbirds and *Drosophila*. *J. exp. Biol.* **56**, 79–104.
WEIS-FOGH, T. (1973). Quick estimates of flight fitness in hovering animals, including novel mechanisms for lift production. *J. exp. Biol.* **59**, 169–230.
WEIS-FOGH, T. (1977). Dimensional analysis of hovering flight. In Pedley (1977), pp. 405–420.
WEIS-FOGH, T. & ALEXANDER R. MCN. (1977). The sustained power output from striated muscle. In Pedley (1977), pp. 511–525.
WITHERS, P. C. & TIMKO, P. L. (1977). The significance of the aerodynamic ground effect to the aerodynamic cost of flight and energetics of the black skimmer (*Rhyncops nigra*). *J. exp. Biol.* **70**, 13–26.